arXiv:1607.04696v3 [hep-ph] 1 Apr 2017

Spectrum and electromagnetic transitions of bottomonium

Wei-Jun Deng, Hui Liu, Long-Cheng Gui * and Xian-Hui Zhong †
1) Department of Physics, Hunan Normal University, Changsha 410081, China
2) Synergetic Innovation Center for Quantum Effects and Applications (SICQEA), Changsha 410081,China and
3) Key Laboratory of Low-Dimensional Quantum Structures and Quantum Control of Ministry of Education, Changsha 410081, China

Stimulated by the exciting progress in the observation of new bottomonium states, we study the bottomonium spectrum. To calculate the mass spectrum, we adopt a nonrelativistic screened potential model. The radial Schrödinger equation is solved with the three-point difference central method, where the spin-dependent potentials are dealt with nonperturbatively. With this treatment, the corrections of the spin-dependent potentials to the wave functions can be included successfully. Furthermore, we calculate the electromagnetic transitions of the nS ($n \leq 4$), nP ($n \leq 3$), and nD ($n \leq 2$) bottomonium states with a nonrelativistic electromagnetic transition operator widely applied to meson photoproduction reactions. Our predicted masses, hyperfine and fine splittings, electromagnetic transition widths and branching ratios of the bottomonium states are in good agreement with the available experimental data. In particular, the EM transitions of $\Upsilon(3S) \to \chi_{b1,2}(1P)\gamma$, which were not well understood in previous studies, can be reasonably explained by considering the corrections of the spin-dependent interactions to the wave functions. We also discuss the observations of the missing bottomonium states by using radiative transitions. Some important radiative decay chains involving the missing bottomonium states are suggested to be observed. We hope our study can provide some useful references to observe and measure the properties of bottomonium mesons in forthcoming experiments.

PACS numbers: 14.40.Pq, 13.20.Gd, 12.39.Jh

I. INTRODUCTION

Heavy quarkonium is considered to be an excellent laboratory to study quantum chromodynamics (QCD) at low energies [1–3]. Due to a large mass of the heavy bottom quark, the bottomonium system is essentially nonrelativistic, which makes it relatively easy for us to study the perturbative and nonperturbative QCD via the bottomonium spectroscopy with a nonrelativistic approximation. In the past few years, great progress has been achieved in the study of the bottomonium spectroscopy [4–7]. A fairly abundant bottomonium spectroscopy has been established in experiments [8](see Tab. I). Furthermore, many new experiments are being and/or to be carried out at LHC and Belle. In near future, more missing bottomonium states will be discovered and more decay channels will be observed in experiments. Thus, it is necessary to carry out a comprehensive study of the bottomonium states according to the recent progress. On the one hand we can obtain more knowledge of bottomonium states from experimental observations. On the other hand, the predicted properties can provide some useful references for our search for the missing bottomonium states in experiments.

In the past years, stimulated by the exciting progress in experiments, many theoretical studies of bottomonium spectrum have been carried out with different methods, such as the widely used potential models [9–17], lattice QCD [18–21], effective Lagrangian approach [22], nonrelativistic effective field theories of QCD [23–25], various coupled-channel quark models [26–28], and light front quark model [29–32]. Although some comparable predictions from different models have been achieved, many properties of the bottomonium states are still not well understood. For example, the recent calculations with the relativized quark model [12] obtain a successful description of the masses for the low-lying excitations, however, the predicted mass for the higher excitation $\Upsilon(6S)$ is about 100 MeV higher than the data if $\Upsilon(11020)$ is identified as $\Upsilon(6S)$; while the recent nonrelativistic constituent quark model [13] gives a good description of the mass of $\Upsilon(6S)$, however, the predicted masses for the ground states $\Upsilon(1S)$ and $\eta_b(1S)$ are about 50 MeV larger than the experimental values. Furthermore, there are puzzles in the electromagnetic (EM) transitions of bottomonium states. For example, about the M1 transitions of $\Upsilon(2S, 3S) \to \eta_b(1S)\gamma$, the predictions from the relativistic quark model [16] and nonrelativistic effective field theories of QCD [25] are about an order of magnitude smaller than the recent predictions from the relativized quark model [12] and nonrelativistic constituent quark model [13]; while about the EM transitions of $\Upsilon(3S) \to \chi_{b1,2}(1P)\gamma$, the predicted partial widths in the literature [11–13] are inconsistent with the data. Thus, to deepen our knowledge about the bottomonium spectrum, more theoretical studies are needed.

In this work, first we use the nonrelativistic screened potential model [11, 33–35] to calculate the masses and wave functions. In this model, the often used linear potential br is replaced with the screened potential $b(1-e^{-\mu r})/\mu$. The reason is that the linear potential, which is expected to be dominant at large distances, is screened or softened by the vacuum polarization effect of the dynamical light quark pairs [36, 37]. Such a screening effect might be important for us to reasonably describe the higher radial and orbital excitations. Considering the corrections of the spin-dependent interactions to the space wave functions cannot be included with the perturbative treatment, we treat the spin-dependent interactions as nonperturbations in our calculations. With the nonperturbative treatment,

*E-mail: guilongcheng@ihep.ac.cn
†E-mail: zhongxh@hunnu.edu.cn

we can reasonably include the effect of spin-dependent interactions on the wave functions, which is important for us to gain reliable predictions of the decays.

Moreover, using the obtained wave functions, we study the EM transitions between bottomonium states. Difference of our method from the often used potential models is that the EM transition operator between initial and final hadron states is used a special nonrelativistic form $h_e \simeq \sum_j [e_j \mathbf{r}_j \cdot \boldsymbol{\epsilon} - \frac{e_j}{2m_j}\boldsymbol{\sigma}_j \cdot (\boldsymbol{\epsilon} \times \hat{\mathbf{k}})] e^{-i\mathbf{k}\cdot\mathbf{r}_j}$ [38], which has been well developed and widely applied to meson photoproduction reactions [39–50]. In this operator, the effect of binding potential between quarks is considered. Furthermore, the possible higher EM multipole contributions to a EM transition process can be included naturally.

The paper is organized as follows. In Sec. II, we calculate the masses and wave functions within a screened potential model. In Sec. III, the EM transitions between the bottomonium states are calculated, and our analysis and discussion are given. Finally, a summary is given in Sec. IV.

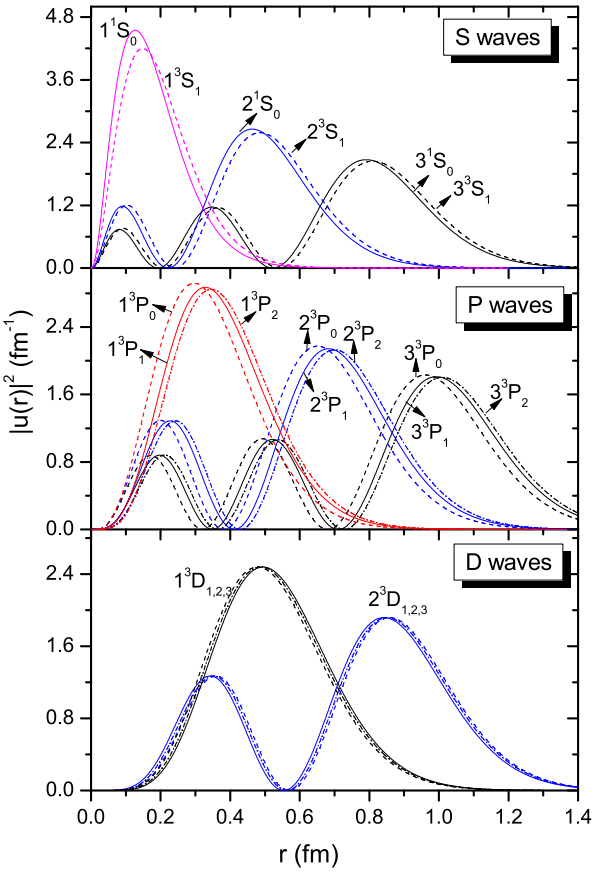


FIG. 1: (Color online) Predicted radial probability density $|u(r)|^2$ for S-, P- and D-wave bottomonium states.

TABLE I: Predicted masses (MeV) of bottomonium states. For comparison, the measured masses (MeV) from the PDG [8], and the theoretical predictions with the previous screened potential model (SNR model) [11], relativized quark model (GI model) [12], and nonrelativistic constituent quark model (NR model) [13] are also listed in the same table.

$n^{2S+1}L_J$	name	J^{PC}	PDG [8]	SNR[11]	GI[12]	NR[13]	Ours
1^3S_1	$\Upsilon(1S)$	1^{--}	9460	9460	9465	9502	9460
1^1S_0	$\eta_b(1S)$	0^{-+}	9398	9389	9402	9455	9390
2^3S_1	$\Upsilon(2S)$	1^{--}	10023	10016	10003	10015	10015
2^1S_0	$\eta_b(2S)$	0^{-+}	9999	9987	9976	9990	9990
3^3S_1	$\Upsilon(3S)$	1^{--}	10355	10351	10354	10349	10343
3^1S_0	$\eta_b(3S)$	0^{-+}		10330	10336	10330	10326
4^3S_1	$\Upsilon(4S)$	1^{--}	10579	10611	10635	10607	10597
4^1S_0	$\eta_b(4S)$	0^{-+}		10595	10623		10584
5^3S_1	$\Upsilon(5S)$	1^{--}	10865	10831	10878	10818	10811
5^1S_0	$\eta_b(5S)$	0^{-+}		10817	10869		10800
6^3S_1	$\Upsilon(6S)$	1^{--}	11020	11023	11102	10995	10997
6^1S_0	$\eta_b(6S)$	0^{-+}		11011	11097		10988
1^3P_2	$\chi_{b2}(1P)$	2^{++}	9912	9918	9897	9886	9921
1^3P_1	$\chi_{b1}(1P)$	1^{++}	9893	9897	9876	9874	9903
1^3P_0	$\chi_{b0}(1P)$	0^{++}	9859	9865	9847	9855	9864
1^1P_1	$h_b(1P)$	1^{+-}	9899	9903	9882	9879	9909
2^3P_2	$\chi_{b2}(2P)$	2^{++}	10269	10269	10261	10246	10264
2^3P_1	$\chi_{b1}(2P)$	1^{++}	10255	10251	10246	10236	10249
2^3P_0	$\chi_{b0}(2P)$	0^{++}	10233	10226	10226	10221	10220
2^1P_1	$h_b(2P)$	1^{+-}	10260	10256	10250	10240	10254
3^3P_2	$\chi_{b2}(3P)$	2^{++}		10540	10550	10521	10528
3^3P_1	$\chi_{b1}(3P)$	1^{++}	10516	10524	10538	10513	10515
3^3P_0	$\chi_{b0}(3P)$	0^{++}		10502	10522	10500	10490
3^1P_1	$h_b(3P)$	1^{+-}		10529	10541	10516	10519
1^3D_3	$\Upsilon_3(1D)$	3^{--}		10156	10155	10127	10157
1^3D_2	$\Upsilon_2(1D)$	2^{--}	10164	10151	10147	10122	10153
1^3D_1	$\Upsilon_1(1D)$	1^{--}		10145	10138	10117	10146
1^1D_2	$\eta_{b2}(1D)$	2^{-+}		10152	10148	10123	10153
2^3D_3	$\Upsilon_3(2D)$	3^{--}		10442	10455	10422	10436
2^3D_2	$\Upsilon_2(2D)$	2^{--}		10438	10449	10418	10432
2^3D_1	$\Upsilon_1(2D)$	1^{--}		10432	10441	10414	10425
2^1D_2	$\eta_{b2}(2D)$	2^{-+}		10439	10450	10419	10432
1^1F_3	$h_{b3}(1F)$	3^{+-}			10355	10322	10339
1^3F_4	$\chi_{b4}(1F)$	4^{++}			10358		10340
1^3F_3	$\chi_{b3}(1F)$	3^{++}			10355	10321	10340
1^3F_2	$\chi_{b2}(1F)$	2^{++}			10350	10315	10338

II. MASS SPECTRUM

As a minimal model of the bottomonium system we use a nonrelativistic screened potential model [11, 33–35]. The effective potential of spin-independent term $V(r)$ is regarded as the sum of Lorentz vector $V_V(r)$ and Lorentz scalar $V_s(r)$ contributions [4], i.e.,

$$V(r) = V_V(r) + V_s(r). \quad (1)$$

TABLE II: Hyperfine and fine splittings in units of MeV for bottomonium in our calculation. The experimental data are taken from the PDG [8]. The theoretical predictions with the previous screened potential model [11], relativized quark model [12], relativistic two-body calculation [14], and nonrelativistic constituent quark model [13, 15] are also listed in the same table for comparison.

Δm	Ours	[11]	[12]	[13]	[14]	[15]	PDG [8]
$m(1^3S_1)$-$m(1^1S_0)$	70	71	63	47	76	49	62.3 ± 3.2
$m(2^3S_1)$-$m(2^1S_0)$	25	29	27	25	38	16	$24.3^{+4.0}_{-4.5}$
$m(3^3S_1)$-$m(3^1S_0)$	17	21	18	19		11	
$m(4^3S_1)$-$m(4^1S_0)$	13	16	12			11	
$m(5^3S_1)$-$m(5^1S_0)$	11	14	9			15	
$m(6^3S_1)$-$m(6^1S_0)$	9	12	5				
$m(1^3P_2)$-$m(1^3P_1)$	18	21	21	12	22	18	19.43 ± 0.57
$m(1^3P_1)$-$m(1^3P_0)$	39	32	29	19	29	48	33.34 ± 0.66
$m(2^3P_2)$-$m(2^3P_1)$	15	18	15	10	18	16	13.19 ± 0.77
$m(2^3P_1)$-$m(2^3P_0)$	29	25	20	15	24	40	22.96 ± 0.84
$m(3^3P_2)$-$m(3^3P_1)$	13	16	12	8		14	
$m(3^3P_1)$-$m(3^3P_0)$	25	22	16	13		36	

For the Lorentz vector potential $V_V(r)$, we adopt the standard color Coulomb form:

$$V_V(r) = -\frac{4}{3}\frac{\alpha_s}{r}. \tag{2}$$

To take into account the screening effects, which might originate from the vacuum polarization of the dynamical light quark pairs [36, 37], we replace the widely used linear scalar potential br with a special form

$$V_s(r) = \frac{b(1-e^{-\mu r})}{\mu}, \tag{3}$$

as suggested in Refs. [11, 33–35]. Here μ is the screening factor which makes the long-range scalar potential of $V_s(r)$ behave like br when $r \ll 1/\mu$, and become a constant b/μ when $r \gg 1/\mu$. The main effect of the screened potential on the spectrum is that the masses of the higher excited states are lowered. Such a screening effect might be important for us to reasonably describe the higher radial and orbital excitations.

We include three spin-dependent potentials as follows. For the spin-spin contact hyperfine potential, we take [51]

$$H_{SS} = \frac{32\pi\alpha_s}{9m_b^2}\tilde{\delta}_\sigma(r)\mathbf{S}_b\cdot\mathbf{S}_{\bar{b}}, \tag{4}$$

where $\mathbf{S}_b$ and $\mathbf{S}_{\bar{b}}$ are spin matrices acting on the spins of the quark and antiquark. We take $\tilde{\delta}_\sigma(r) = (\sigma/\sqrt{\pi})^3 e^{-\sigma^2 r^2}$ as in Ref. [51]. The five parameters in the above equations (α_s, b, μ, m_b, σ) are determined by fitting the spectrum.

For the spin-orbit term and the tensor term, we take the common forms [4]:

$$H_{SL} = \frac{1}{2m_b^2 r}\left(3\frac{dV_V}{dr} - \frac{dV_s}{dr}\right)\mathbf{L}\cdot\mathbf{S}, \tag{5}$$

and

$$H_T = \frac{1}{12m_b^2}\left(\frac{1}{r}\frac{dV_V}{dr} - \frac{d^2V_V}{dr^2}\right)S_T, \tag{6}$$

where $\mathbf{L}$ is the relative orbital angular momentum of b and $\bar{b}$ quarks, $\mathbf{S} = \mathbf{S}_b + \mathbf{S}_{\bar{b}}$ is the total quark spin, and the spin tensor S_T is defined by [4]

$$S_T = 6\frac{\mathbf{S}\cdot\mathbf{r}\mathbf{S}\cdot\mathbf{r}}{r^2} - 2\mathbf{S}^2. \tag{7}$$

In the $|^{2S+1}L_J\rangle$ basis, the matrix element for the spin-spin operator $\mathbf{S}_b\cdot\mathbf{S}_{\bar{b}}$ is

$$\langle\mathbf{S}_b\cdot\mathbf{S}_{\bar{b}}\rangle = \frac{1}{2}S(S+1) - \frac{3}{4}. \tag{8}$$

For the spin-orbit operator $\mathbf{L}\cdot\mathbf{S}$, its matrix element is

$$\langle\mathbf{L}\cdot\mathbf{S}\rangle = \frac{1}{2}[J(J+1) - L(L+1) - S(S+1)]. \tag{9}$$

The element of the tensor operator S_T can be written in the form [52]

$$\langle S_T\rangle = \frac{4\langle\mathbf{S}^2\mathbf{L}^2 - \frac{3}{2}\mathbf{L}\cdot\mathbf{S} - 3(\mathbf{L}\cdot\mathbf{S})^2\rangle}{(2L+3)(2L-1)}. \tag{10}$$

To obtain masses and wave functions of the bottomonium states, we need to solve the radial Schrödinger equation

$$\frac{d^2u(r)}{dr^2} + 2\mu_R\left[E - V_{b\bar{b}}(r) - \frac{L(L+1)}{2\mu_R r^2}\right]u(r) = 0, \tag{11}$$

with

$$V_{b\bar{b}}(r) = V(r) + H_{SS} + H_{SL} + H_T, \tag{12}$$

where $\mu_R = m_b m_{\bar{b}}/(m_b + m_{\bar{b}})$ is the reduced mass of the system, and E is the binding energy of the system. Then, the mass of a $b\bar{b}$ state is obtained by

$$M_{b\bar{b}} = 2m_b + E. \tag{13}$$

In the literature, the spin-dependent interactions were usually dealt with perturbatively. Although the meson mass obtains perturbative corrections from these spin-dependent potentials, the wave functions obtain no corrections from these spin-dependent potentials. To reasonably include the corrections from these spin-dependent potentials to both the mass and wave function of a meson state, we deal with the spin-dependent interactions nonperturbatively.

In this work, we solve the radial Schrödinger equation by using the three-point difference central method [53] from central ($r = 0$) towards outside ($r \to \infty$) point by point. In this method, we need to know the role of $u(r \to 0)$. When $r \to 0$ we easily obtain $u(r \to 0) \propto r^{L+1}$ if we neglect the contributions of the spin-orbit and tensor terms. However, including the spin-orbit and tensor potential contributions, we have a term $\propto 1/r^3$ in the potential. In the limit $r \to 0$, the potential $V_{b\bar{b}}(r) \propto 1/r^3$. In this case, we do not know the role of

$u(r \to 0)$, thus, we cannot solve the radial Schrödinger equation with the three-point differential central method. To overcome this problem, we assume that in a small range $r \in (0, r_c)$, the $V_{b\bar{b}}(r) \propto 1/r_c^3$, which is a finite constant. Then, the role of $u(r \to 0)$ is still $\propto r^{L+1}$. The price of our method is that a cutoff distance r_c should be introduced in the calculation, which is determined by fitting the spectrum. The details of the method for solving Eq.(11) are outlined in the Appendix.

For the model parameters, we take $\alpha_s = 0.368(3)$, $b = 0.206(2)$ GeV^2, $\mu = 0.056(11)$ GeV, $m_b = 4.757(2)$ GeV, and $\sigma = 3.10(25)$ GeV. This parameter set is slightly different from that suggested in Ref. [11]. In our calculation, the cutoff distance $r_c = 0.060(12)$ fm is adopted. The uncertainties for these determined parameters mean that if one changes one of the parameter within its uncertainty, the mass change of one state is less than 5 MeV. It should be mentioned that the masses of the $^3P_0$ states are sensitive to the cutoff distance r_c. Thus, in the present work we use the mass of $\chi_{b0}(1P)$ to determine the cutoff distance r_c. With the determined cutoff distance $r_c = 0.06$ fm, the calculated masses of the other $^3P_0$ states are in good agreement with the measurements and the other model predictions.

With the determined parameter set, by solving the radial Schrödinger equation we obtain the masses of the bottomonium states, which have been listed in Tab I. From the table, we see that our results are compatible with the previous screened potential model predictions [11], which indicates that our numerical method is reliable. The recent relativized quark model can successfully describe the low-lying bottomonium states, however, their predicted mass for the higher excitations $\Upsilon(6S)$ is about 100 MeV larger than the experimental measurements [12]. Although the recent nonrelativistic constituent quark model systematically improve the descriptions of the higher mass spectrum, the predicted masses for the ground states $\Upsilon(1S)$ and $\eta_b(1S)$ are about $40 \sim 50$ MeV higher than the data [13]. Interestedly, it is found that the screened potential model obtains a fairly good description of the masses not only for the low-lying states, but also for the higher excitation $\Upsilon(6S)$.

Furthermore, in Tab. II, we give our predictions of the hyperfine splittings for some S-wave states, and fine splittings for some P-wave states. It is found that our predicted splittings are in good agreement with the world average data [8]. Comparing the model predictions [11–15] with each other, we find obvious model dependencies of the predicted mass splittings. Thus, to better understand these nonperturbative strong interactions in the bottomonium system, more model-independent studies are needed.

In order to clearly see the properties of the wave functions, we plot the radial probability density of the states as a function of the interquark distance r in Fig. 1. It is found that the spin-dependent potentials have notable corrections to the S- and triplet P-wave states; however, the corrections to the triplet D-wave states are tiny. The strong attractive spin-spin potential H_{SS} shifts the wave functions of the $^1S_0$ states towards the center, while the strong attractive tensor potential H_T shifts the wave functions of the $^3P_{0,1}$ states towards the center.

III. ELECTROMAGNETIC TRANSITIONS

Using these obtained wave functions of the bottomonium states, we further study their EM transitions. The quark-photon EM coupling at the tree level is adopted as

$$H_e = -\sum_j e_j \bar{\psi}_j \gamma_\mu^j A^\mu(\mathbf{k}, \mathbf{r}) \psi_j, \tag{14}$$

where ψ_j stands for the jth quark field in a hadron. The photon has three momentum $\mathbf{k}$, and the constituent quark ψ_j carries a charge e_j.

To match the nonrelativistic wave functions of the bottomonium states, we should adopt the nonrelativistic form of Eq. (14) in the calculations. For the EM transition of a hadron, in the initial-hadron-rest system the nonrelativistic expansion of H_e in Eq.(14) becomes [38, 41]

$$h_e \simeq \sum_j \left[e_j \mathbf{r}_j \cdot \boldsymbol{\epsilon} - \frac{e_j}{2m_j} \boldsymbol{\sigma}_j \cdot (\boldsymbol{\epsilon} \times \hat{\mathbf{k}}) \right] \phi, \tag{15}$$

where m_j, $\boldsymbol{\sigma}_j$, and $\mathbf{r}_j$ stand for the constituent mass, Pauli spin vector, and coordinate for the jth quark, respectively. The vector $\boldsymbol{\epsilon}$ is the polarization vector of the photon. For emitting a photon, we have $\phi = e^{-i\mathbf{k}\cdot\mathbf{r}_j}$, while for absorbing a photon, we have $\phi = e^{+i\mathbf{k}\cdot\mathbf{r}_j}$. It is found that the first and second terms in Eq.(15) are responsible for the electric and magnetic transitions, respectively. The main feature of this EM transition operator is that the effects of binding potential between quarks are considered. Furthermore, the possible higher EM multipole contributions are included naturally. This nonrelativistic form has been widely applied to meson photoproduction reactions [39–50]. It should be mentioned that, at the order of $1/m_j$, we have neglected the contributions from the term $e_j \mathbf{r}_j \cdot \boldsymbol{\epsilon} \mathbf{p}_j \cdot \hat{\mathbf{k}}/m_j$ as suggested in Refs. [39, 40] for a strong suppression of $\mathbf{p}_j \cdot \hat{\mathbf{k}}/m_j$.

Then, one obtains the standard helicity amplitude $\mathcal{A}$ of the radiative decay process by the relation

$$\mathcal{A} = -i\sqrt{\frac{\omega_\gamma}{2}} \langle f|h_e|i\rangle. \tag{16}$$

Finally, we can calculate the EM decay width by

$$\Gamma = \frac{|\mathbf{k}|^2}{\pi} \frac{2}{2J_i+1} \frac{M_f}{M_i} \sum_{J_{fz},J_{iz}} |\mathcal{A}_{J_{fz},J_{iz}}|^2, \tag{17}$$

where J_i is the total angular momentum of an initial meson and J_{fz} and J_{iz} are the components of the total angular momenta along the z axis of initial and final mesons, respectively. In our calculation, for the well-established bottomonium states, the experimental masses are adopted [8]; while for the missing bottomonium states, their masses are adopted from our theoretical predictions.

A. $\Upsilon(1S) \to \eta_b(1S)\gamma$

The $\Upsilon(1S) \to \eta_b(1S)\gamma$ decay process is a typical M1 transition at tree level, which is strongly suppressed by the constituent bottom quark mass m_b. Our predicted partial width

TABLE III: Partial widths of the M1 radiative transitions for some low-lying S- and P-wave bottomonium states. For comparison, the measured values from the PDG [8], and the theoretical predictions with the relativistic quark model [16], nonrelativistic effective field theories of QCD (EFT model) [25], relativized quark model (GI model) [12], and nonrelativistic constituent quark model (NR model) [13] are also listed in the same table.

Initial meson	Final meson	E_γ (MeV)			Γ_{M1} (eV)					Γ_{M1} (eV)
state	state	Ref.[16]	GI [12]	ours	Ref.[16]	GI [12]	EFT [25]	NR [13]	Ours	PDG [8]
$\Upsilon(1^3S_1)$	$\eta_b(1^1S_0)$	60	62	62	5.8	10	15.2	9.34	10	
$\Upsilon(2^3S_1)$	$\eta_b(2^1S_0)$	33	24	24	1.4	0.59	0.67	0.58	0.59	
	$\eta_b(1^1S_0)$	604	606	606	6.4	81	6^{+26}_{-6}	56.5	66	12.5 ± 4.9
$\eta_b(2^1S_0)$	$\Upsilon(1^3S_1)$	516	524	524	12	68	~ 80	45.0	64	
$\Upsilon(3^3S_1)$	$\eta_b(3^1S_0)$	27	18	18	0.8	0.25		0.66	3.9	
	$\eta_b(2^1S_0)$	359	350	350	1.5	0.19		11.0	11	< 14
	$\eta_b(1^1S_0)$	911	913	913	11	60		57.0	71	10 ± 2
$\eta_b(3^1S_0)$	$\Upsilon(2^3S_1)$	301	309	309	2.8	9.1		9.20	8.7	
	$\Upsilon(1^3S_1)$	831	840	840	24	74		51.0	60	
$\chi_{b2}(1^3P_2)$	$h_b(1^1P_1)$		13	13		9.6×10^{-2}	0.12	8.9×10^{-2}	9.5×10^{-2}	
$h_b(1^1P_1)$	$\chi_{b1}(1^3P_1)$		6	6		1.0×10^{-2}	9.0×10^{-3}	1.15×10^{-2}	9.4×10^{-3}	
	$\chi_{b0}(1^3P_0)$		40	40		0.89	0.96	0.86	0.90	
$\chi_{b2}(2^3P_2)$	$h_b(1^1P_1)$		363	363		0.24		1.78	4.5	
$\chi_{b1}(2^3P_1)$			350	350		2.2		0.17	0.18	
$\chi_{b0}(2^3P_0)$			329	329		9.7		2.39	16	
$h_b(2^1P_1)$	$\chi_{b2}(1^3P_2)$		342	342		2.2		6.91×10^{-3}	1.1	
	$\chi_{b1}(1^3P_1)$		360	360		1.1		1.28	2.5	
	$\chi_{b0}(1^3P_0)$		393	393		0.32		36.4	10	

is

$$\Gamma[\Upsilon(1S) \to \eta_b(1S)\gamma] \simeq 10\,\text{eV}. \tag{18}$$

Combining this partial width with the measured total width of $\Upsilon(1S)$ [8], we obtain

$$\mathcal{B}[\Upsilon(1S) \to \eta_b(1S)\gamma] \simeq 2.0\times10^{-4}. \tag{19}$$

Our predictions are in good agreement with the recent results of the relativized quark model [12] and nonrelativistic constituent quark model [13] (see Tab. III). However, our predicted $\Gamma[\Upsilon(1S) \to \eta_b(1S)\gamma]$ is larger than the value 5.8 eV from the relativistic quark model [16], while smaller than the recent prediction 15.2 eV from the pNRQCD approach [25]. It should be mentioned that this decay rate is extremely sensitive to the masses of $\Upsilon(1S)$ and $\eta_b(1S)$. If all of the models adopt the experimental masses, the predictions of $\Gamma[\Upsilon(1S) \to \eta_b(1S)\gamma]$ from different models might be consistent with each other.

B. Radiative transitions of $2S$ states

1. $\Upsilon(2S)$

The allowed EM transitions of $\Upsilon(2S)$ are $\Upsilon(2S) \to \chi_{bJ}(1P)\gamma$ and $\Upsilon(2S) \to \eta_b(1S,2S)\,\gamma$. The $\Upsilon(2S) \to \chi_{bJ}(1P)\gamma$ processes are governed by the E1 transitions, while $\Upsilon(2S) \to \eta_b(1S,2S)\,\gamma$ are typical M1 transitions.

From Tab. IV, it is found that our predicted partial decay widths for the $\Upsilon(2S) \to \chi_{bJ}(1P)\gamma$ processes are in good agreement with the world average data from the PDG [8], and also are consistent with predictions from various potential models [11–16].

For the M1 transitions $\Upsilon(2S) \to \eta_b(1S,2S)\gamma$, our predicted partial decay widths have been listed in Tab. III. From the table, it is seen that our predicted $\Gamma[\Upsilon(2S) \to \eta_b(2S)\gamma]$ is in agreement with the other model predictions. It should be pointed out that although our predicted $\Gamma[\Upsilon(2S) \to \eta_b(1S)\gamma]$ is compatible with the recent potential model predictions [12, 13], it is about 5 times larger than the average value $1.25(49)\times10^{-2}$ keV from the PDG [8] and the recent lattice NRQCD result $1.72(55)\times10^{-2}$ keV [18]. More studies of the M1 transition $\Upsilon(2S) \to \eta_b(1S)\gamma$ are needed in both theory and experiments.

2. $\eta_b(2S)$

The $\eta_b(2S)$ resonance can decay into $h_b(1P)\gamma$ and $\Upsilon(1S)\gamma$ channels by the E1 and M1 transitions, respectively. Our predicted partial decay width of $\Gamma[\eta_b(2S) \to h_b(1P)\gamma] \simeq 3.41$ keV is in good agreement with the predictions of the relativistic quark model [16], potential model [12], and nonrelativistic constituent quark model [13] (see Tab. IV). However, it is about a factor 1.8 smaller than the previous SNR model prediction [11]. This difference might come from the corrections of the spin-dependent potentials to the wave function of

$\eta_b(2S)$.

Furthermore, from Tab. III it is seen that our predicted partial decay width for the M1 transition $\eta_b(2S) \to \Upsilon(1S)\gamma$ is compatible with the recent predictions of potential models [12, 13], and with the pNRQCD approach [25]. However, our prediction is notably larger than $\Gamma[\eta_b(2S) \to \Upsilon(1S)\gamma] \simeq 12$ eV predicted with a relativistic quark model [16] (see Tab. III).

C. Radiative transitions of $1P$ states

The typical radiative transitions of $\chi_{bJ}(1P)$ are $\chi_{bJ}(1P) \to \Upsilon(1S)\gamma$. From the Tab. V, it is found that the partial widths $\Gamma[\chi_{bJ}(1P) \to \Upsilon(1S)\gamma]$ predicted by us are in agreement with the predictions in [11–13, 15, 16]. Combining our predicted partial widths with the measured branching ratios $\mathcal{B}[\chi_{b0}(1P) \to \Upsilon(1S)\gamma] \simeq (1.76 \pm 0.48)\%$, $\mathcal{B}[\chi_{b1}(1P) \to \Upsilon(1S)\gamma] \simeq (33.9 \pm 2.2)\%$, and $\mathcal{B}[\chi_{b2}(1P) \to \Upsilon(1S)\gamma] \simeq (19.1 \pm 1.2)\%$ [8], we easily estimate the total widths for $\chi_{b0}(1P)$, $\chi_{b1}(1P)$ and $\chi_{b2}(1P)$, which are

$$\Gamma^{\rm total}_{\chi_{b0}(1P)} \simeq 1.56^{+0.59}_{-0.33}\,{\rm MeV}, \quad (20)$$

$$\Gamma^{\rm total}_{\chi_{b1}(1P)} \simeq 94 \pm 7\,{\rm keV}, \quad (21)$$

$$\Gamma^{\rm total}_{\chi_{b2}(1P)} \simeq 166^{+12}_{-9}\,{\rm keV}, \quad (22)$$

respectively. It is interesting to find that the estimated width for $\chi_{b0}(1P)$ is consistent with the recent measurement 1.3 ± 0.9 MeV from the Belle Collaboration [54]. It should be mentioned that these widths predicted by us strongly depend on the measured branching ratios. It is found that $\mathcal{B}[\chi_{b0}(1P) \to \Upsilon(1S)\gamma]$ still bears a large uncertainty. Thus, to determine finally the width of $\chi_{b0}(1P)$, more accurate measurements are needed.

For the singlet state $h_b(1P)$, its main radiative transition is $h_b(1P) \to \eta_b(1S)\gamma$. We predict that $\Gamma[h_b(1P) \to \eta_b(1S)\gamma] \simeq 35.8$ keV, which is consistent with the predictions in Refs. [11, 12] (see Tab. V). A relatively large partial width was also predicted in Ref [16]. Combining the measured branching ratio $\mathcal{B}[h_b(1P) \to \eta_b\gamma] \simeq 49^{+8}_{-7}\%$ [8] with our predicted partial width, we estimate that the total width of $h_b(1P)$ might be

$$\Gamma^{\rm total}_{h_b(1P)} \simeq 73^{+12}_{-10}\ {\rm keV}, \quad (23)$$

which could be tested in future experiments.

Finally, we give our estimations of the typical M1 transitions $h_b(1P) \to \chi_{b0,1}(1P)\gamma$, which are listed in Tab. III. The rates of these M1 transitions are very weak. Our results are consistent with those obtained in the framework of the relativized quark model [12] and nonrelativistic constituent quark model [13].

D. Radiative transitions of $1D$ states

In the $1D$ bottomonium states, only the 2^{--} state $\Upsilon_2(1D)$ with a mass of $M_{\Upsilon_2(1D)} = 10164$ MeV is confirmed in experiments [55]. The other $1D$ states are still missing. The discovery of the $\Upsilon_2(1D)$ state provides a strong constrain on the masses of the other $1D$ states. In our calculations, we predict the mass splittings $M_{\Upsilon_3(1D)} - M_{\Upsilon_2(1D)} \simeq 4$, $M_{\Upsilon_2(1D)} - M_{\Upsilon_1(1D)} \simeq 7$, and $M_{\Upsilon_2(1D)} - M_{\eta_{b2}(1D)} \simeq 0$ MeV. Combining these predicted multiplet mass splittings with the measured mass of $M_{\Upsilon_2(1D)} = 10164$ MeV, one can predict the masses for the $\Upsilon_1(1D)$, $\Upsilon_3(1D)$ and $\eta_{b2}(1D)$ states, which are $M_{\Upsilon_1(1D)} \simeq 10157$ MeV, $M_{\Upsilon_3(1D)} \simeq 10168$ MeV, and $M_{\eta_{b2}(1D)} \simeq 10164$ MeV, respectively.

1. $\Upsilon_2(1D)$

For the established 2^{--} state $\Upsilon_2(1D)$ [i.e., $\Upsilon_2(10164)$], the EM transitions are dominated by $\Upsilon_2(1D) \to \chi_{b1,2}(1P)\gamma$. We calculate their partial decay widths, which are listed in Tab. V. Combining with the predicted partial widths of $\Gamma[\Upsilon_2(1D) \to ggg] \simeq 0.62$ keV and $\Gamma[\Upsilon_2(1D) \to \pi\pi\Upsilon(1S)] \simeq 0.29$ keV from Ref. [13], we estimate the total width of $\Upsilon_2(1D)$, $\Gamma_{\rm tot} \simeq 30$ keV. With this estimated width, we further predict the branching ratios

$$\mathcal{B}[\Upsilon_2(1D) \to \chi_{b1}(1P)\gamma] \simeq 73\%, \quad (24)$$

$$\mathcal{B}[\Upsilon_2(1D) \to \chi_{b2}(1P)\gamma] \simeq 24\%. \quad (25)$$

Our results are in agreement with the predictions obtained with the previous SNR model [11], relativistic quark model [16], and nonrelativistic constituent quark model [13]. The large branching ratios indicate the $\Upsilon_2(1D) \to \chi_{b1,2}(1P)\gamma$ transitions may be observed in forthcoming experiments.

2. *The missing* $1D$ *states*

According to the predicted mass $M_{\Upsilon_1(1D)} = 10157$ MeV of $\Upsilon_1(1D)$, we calculate the partial decay widths of $\Gamma[\Upsilon_1(1D) \to \chi_{b0,1,2}(1P)\gamma]$, which are listed in Tab. V. In Ref. [13], the total width of $\Upsilon_1(1D)$ is predicted to be $\Gamma_{\rm tot} \simeq 44$ keV. Using it as an input, we predict

$$\mathcal{B}[\Upsilon_1(1D) \to \chi_{b0}(1P)\gamma] \simeq 45\%, \quad (26)$$

$$\mathcal{B}[\Upsilon_1(1D) \to \chi_{b1}(1P)\gamma] \simeq 30\%, \quad (27)$$

$$\mathcal{B}[\Upsilon_1(1D) \to \chi_{b2}(1P)\gamma] \simeq 2\%. \quad (28)$$

These branching ratios are consistent with those from the recent works [12, 13]. The fairly large branching ratios indicate that the missing $\Upsilon_1(1D)$ state is most likely to be observed through the radiative transitions $\Upsilon_1(1D) \to \chi_{b0,1}(1P)\gamma$.

While taking the mass of $\Upsilon_3(1D)$ with $M_{\Upsilon_3(1D)} = 10168$ MeV, we calculate the partial decay widths of $\Gamma[\Upsilon_3(1^3D_3) \to \chi_{bJ}(1P)\gamma]$. Our results are listed in Tab. V. It is found that the EM decays of $\Upsilon_3(1D)$ are governed by the $\chi_{b2}(1P)\gamma$ channel, and the decay rates into the $\chi_{b0,1}(1P)\gamma$ channels are negligibly small. Our prediction of $\Gamma[\Upsilon_3(1D) \to \chi_{b2}(1P)\gamma] \simeq 32.1$ keV is consistent with the predictions from the potential models [11, 12] and relativistic quark model [16] (see Tab. V). According to the predictions in Refs. [12, 13], the partial

widths of $\Gamma[\Upsilon_2(1D) \to ggg]$ and $\Gamma[\Upsilon_2(1D) \to \pi\pi\Upsilon(1S)]$ are too small to compare with $\Gamma[\Upsilon_3(1D) \to \chi_{b2}(1P)\gamma]$, thus, the branching fraction of $\mathcal{B}[\Upsilon_3(1D) \to \chi_{b2}(1P)\gamma] \sim 100\%$. To establish $\Upsilon_3(1D)$, the decay channel $\chi_{b2}(1P)\gamma$ is worth observing in future experiments.

For the singlet $1D$ state $\eta_{b2}(1D)$, our predicted partial width $\Gamma[\eta_{b2}(1D) \to h_b(1P)\gamma] \simeq 30.3$ keV is close to the predictions from the other potential models [11, 12, 16] (see Tab. V). Combining with the predictions $\Gamma[\eta_{b2}(1D) \to gg] \simeq 1.8$ keV and $\Gamma[\eta_{b2}(1D) \to \pi\pi\eta_b(1S)] \simeq 0.35$ keV in Ref. [12], we obtain the total width of $\Upsilon_1(1D)$, $\Gamma_{\rm tot} \simeq 32.5$ keV, with which we further estimate that

$$\mathcal{B}[\eta_{b2}(1D) \to h_b(1P)\gamma] \simeq 93\%. \quad (29)$$

The large radiative transition rate indicates that the missing $\eta_{b2}(1D)$ state is most likely to be observed in the $h_b(1P)\gamma$ channel.

E. Radiative transitions of $2P$ states

The $2P$ bottomonium states have been established in experiments. The branching ratios of $\mathcal{B}[\chi_{b0,1,2}(2P) \to \Upsilon(1S, 2S)\gamma]$ and $\mathcal{B}[h_b(2P) \to \eta_b(1S, 2S)\gamma]$ have been measured. These measured branching ratios give us a good chance to study the radiative transitions of the $2P$ bottomonium states, and test our model.

1. $\chi_{b0}(2P)$

The allowed EM decay modes of $\chi_{b0}(2P)$ are $\Upsilon(1S, 2S)\gamma$, $\Upsilon_1(1D)\gamma$ and $h_b(1P)\gamma$. We calculate their partial widths and list them in Tab. IV. From the table, one can see that our predictions are compatible with the other model predictions. Taking the predicted total width $\Gamma_{\rm tot} \simeq 2.5$ MeV of $\chi_{b0}(2P)$ from Ref. [12] as an input, we further predict that

$$\mathcal{B}[\chi_{b0}(2P) \to \Upsilon(1S)\gamma] \simeq 2.2 \times 10^{-3}, \quad (30)$$
$$\mathcal{B}[\chi_{b0}(2P) \to \Upsilon(2S)\gamma] \simeq 5.8 \times 10^{-3}. \quad (31)$$

Our prediction is compatible with the recent results obtained from potential models [12, 13], and the previous results obtained from $\rm SNR_1$ model [11]. However, the predicted branching ratio $\mathcal{B}[\chi_{b0}(2P) \to \Upsilon(2S)\gamma]$ is about an order of magnitude smaller than the data from the PDG [8]. To test our predictions, more accurate measurements are needed in experiments.

We also study the typical M1 transition $\chi_{b0}(2P) \to h_b(1P)\gamma$. Our predicted partial decay width $\Gamma[\chi_{b0}(2P) \to h_b(1P)\gamma] \simeq 1.6 \times 10^{-2}$ keV is close to the recent predictions with the GI potential model [12] (see Tab. III).

2. $\chi_{b1}(2P)$

The $\chi_{b1}(2P)$ state can decay into $\Upsilon(1S, 2S)\gamma$, $\Upsilon(1^3D_{2,3})\gamma$ and $h_b(1P)\gamma$ via radiative transitions. Our predicted partial widths for these transitions are listed in Tab. IV. From the table it is found that the decay rates of $\chi_{b1}(2P)$ into the D-wave states $\Upsilon_{1,2}(1D)$ are much weaker than those into the S-wave states. Our predicted partial widths of $\Gamma[\chi_{b1}(2P) \to \Upsilon(1S, 2S)\gamma]$ are consistent with observations from the CLEO Collaboration [56]. Combining our predicted partial widths with the total width $\Gamma_{\rm tot} \simeq 133$ keV predicted in Ref. [13], we obtain that

$$\mathcal{B}[\chi_{b1}(2P) \to \Upsilon(1S)\gamma] \simeq 8.1\%, \quad (32)$$
$$\mathcal{B}[\chi_{b1}(2P) \to \Upsilon(2S)\gamma] \simeq 11.5\%, \quad (33)$$

which are close to the measured values $\mathcal{B}[\chi_{b1}(2P) \to \Upsilon(1S)\gamma] \simeq 9.2 \pm 0.8\%$ and $\mathcal{B}[\chi_{b1}(2P) \to \Upsilon(2S)\gamma] \simeq 19.9 \pm 1.9\%$ [8]. The branching fraction ratio

$$\frac{\Gamma[\chi_{b1}(2P) \to \Upsilon(2S)\gamma]}{\Gamma[\chi_{b1}(2P) \to \Upsilon(1S)\gamma]} \simeq 1.4, \quad (34)$$

is slightly smaller than the world average value 2.2 ± 0.4 from the PDG [8]. From Tab. IV, we can find that this ratio has a strong model dependency. To test the predictions from various models, more accurate measurements are needed in experiments.

Furthermore, the typical M1 transition $\chi_{b2}(2P) \to h_b(1P)\gamma$ is also studied. The predicted partial decay width

$$\Gamma[\chi_{b2}(2P) \to h_b(1P)\gamma] \simeq 1.8 \times 10^{-4} \text{ keV}, \quad (35)$$

is about an order of magnitude smaller than the recent prediction 2.2×10^{-3} keV in Ref. [12]. However, the recent prediction 1.7×10^{-4} keV with a nonrelativistic constituent quark model [13] is in good agreement with our prediction. The Lattice QCD study may be able to clarify this puzzle.

3. $\chi_{b2}(2P)$

The $\chi_{b2}(2P)$ state can decay into $\Upsilon(1S, 2S)\gamma$, $\Upsilon_{1,2,3}(1D)\gamma$ and $h_b(1P)\gamma$ channels. In these decays, the $\chi_{b2}(2P) \to \Upsilon(1S, 2S)\gamma$ processes play dominant roles. From Tab. IV, it is seen that our predicted partial widths of $\Gamma[\chi_{b2}(2P) \to \Upsilon(1S, 2S)\gamma]$ are compatible with the observations from the CLEO Collaboration [56] and other model predictions [11–13, 16]. Combining our predicted partial widths with the estimated total width of $\chi_{b2}(2P)$ according to the CLEO observations [56], i.e., $\Gamma_{\rm tot} \simeq 143$ keV, we have

$$\mathcal{B}[\chi_{b2}(2P) \to \Upsilon(1S)\gamma] \simeq 9.5\%, \quad (36)$$
$$\mathcal{B}[\chi_{b2}(2P) \to \Upsilon(2S)\gamma] \simeq 11\%, \quad (37)$$

which are close to the average data from the PDG [8]. The estimated partial width ratio

$$\frac{\Gamma[\chi_{b2}(2P) \to \Upsilon(2S)\gamma]}{\Gamma[\chi_{b2}(2P) \to \Upsilon(1S)\gamma]} \simeq 1.2, \quad (38)$$

is also close to the lower limit of the world average data $1.51^{+0.59}_{-0.47}$ from the PDG [8]. This ratio has strong model dependencies. Thus, more accurate measurements are needed to test various model predictions.

The decay rates of $\chi_{b2}(2P) \to \Upsilon_{1,2,3}(1D)\gamma$ are much weaker than those of $\chi_{b2}(2P) \to \Upsilon(1S, 2S)\gamma$. Our predicted results are close to the predictions in Refs. [11, 13, 16] (see Tab. IV). Combining the estimated total width of $\chi_{b2}(2P)$ with our predicted partial widths, we have

$$\mathcal{B}[\chi_{b2}(2P) \to \Upsilon_1(1D)\gamma] \simeq 1.8 \times 10^{-4}, \quad (39)$$
$$\mathcal{B}[\chi_{b2}(2P) \to \Upsilon_2(1D)\gamma] \simeq 2.9 \times 10^{-3}, \quad (40)$$
$$\mathcal{B}[\chi_{b2}(2P) \to \Upsilon_3(1D)\gamma] \simeq 1.7 \times 10^{-2}. \quad (41)$$

To look for the missing $\Upsilon_3(1D)$ state, the three-photon decay chain $\chi_{b2}(2P) \to \Upsilon_3(1D)\gamma \to \chi_{b2}(1P)\gamma\gamma \to \Upsilon(1S)\gamma\gamma\gamma$ is worth observing. The combined branching ratio can reach up to $O(10^{-3})$.

4. $h_b(2P)$

The $h_b(2P)$ state can decay into $\eta_b(1S, 2S)\gamma$, $\eta_{b2}(1D)\gamma$, and $\chi_{b0,1,2}(1P)\gamma$ via EM transitions, in which the $\eta_b(1S, 2S)\gamma$ decay modes are dominant. We calculate the partial decay widths of $\Gamma[h_b(2P) \to \eta_b(1S, 2S)\gamma]$, which are listed in Tab. IV. Our results are compatible with the other model predictions [11–13, 16]. Our predicted partial width ratio,

$$\frac{\Gamma[h_b(2P) \to \eta_b(2S)\gamma]}{\Gamma[h_b(2P) \to \eta_b(1S)\gamma]} \simeq 1.0, \quad (42)$$

is close to the lower limit of the measurement 1.0 ± 4.3 from the Belle Collaboration [57]. Furthermore, combining the measured branching ratio $\mathcal{B}[h_b(2P) \to \eta_b(1S)\gamma] \simeq 22.3 \pm 3.8^{+3.1}_{-3.3}\%$ with our predicted partial width, we estimate the total width of $h_b(1P)$, which is

$$\Gamma^{\rm total}_{h_b(2P)} \simeq 72^{+34}_{-17} \text{ keV}. \quad (43)$$

It could be tested in future experiments.

We also study the transition of $h_b(2P) \to \eta_{b2}(1D)\gamma$. The predicted partial width $\Gamma[h_b(2P) \to \eta_{b2}(1D)\gamma] \simeq 2.24$ keV is compatible with the predictions from the relativized quark model [12] and the relativistic quark model [16]. Using this predicted total width in Eq. (43) as an input, we further predict

$$\mathcal{B}[h_b(2P) \to \eta_{b2}(1D)\gamma] \simeq 3\%. \quad (44)$$

Combining this ratio with our predicted ratio of $\mathcal{B}[\eta_{b2}(1D) \to h_b(1P)\gamma] \simeq 93\%$ and the measured ratios of $\mathcal{B}[h_b(1P) \to \eta_b\gamma] \simeq 49\%$, we obtain the combined branching ratio for the three-photon cascade $h_b(2P) \to \eta_{b2}(1D)\gamma \to h_b(1P)\gamma\gamma \to \eta_b\gamma\gamma\gamma$:

$$\mathcal{B}[h_b(2P) \to \eta_{b2}(1D)\gamma \to h_b(1P)\gamma\gamma \to \eta_b\gamma\gamma\gamma] \simeq 1.4\%. \quad (45)$$

Thus, to establish the missing $\eta_{b2}(1D)$ this three-photon cascade is worth observing.

Finally, we give our predictions for the typical M1 transitions $h_b(2P) \to \chi_{b0,1,2}(1P)\gamma$. Our results are listed in Tab. III. It is seen that concerning these M1 transitions, there are obvious differences in various model predictions.

F. Radiative transitions of $3S$ states

1. $\Upsilon(3S)$

$\Upsilon(3S)$ is well established in experiments. Its mass and width are $M_{\Upsilon(3S)} = 10355.2 \pm 0.5$ MeV and $\Gamma = 20.32 \pm 1.85$ keV, respectively. The EM transitions $\Upsilon(3S) \to \chi_{bJ}(1P, 2P)\gamma$ and $\Upsilon(3S) \to \eta_b(1S, 2S)\gamma$ have been observed in experiments. We calculate the partial widths and compare them with the data in Tab. IV.

From the table, it is found that for the EM transitions $\Upsilon(3S) \to \chi_{bJ}(1P)\gamma$, the predicted partial widths are in good agreement with the world average data from the PDG [8]. Note that the transition widths for $\Upsilon(3S) \to \chi_{b1,2}(1P)\gamma$ calculated from the previous screened potential model [11] are too large as compared with experimental data. These problems have been overcome in our calculations by considering the corrections of the spin-dependent interactions to the wave functions. It indicates that the corrections of the spin-dependent interactions to the wave functions are important to understand these EM transitions, which was also found in Ref. [58].

While for the EM transitions $\Upsilon(3S) \to \chi_{bJ}(2P)\gamma$, from Tab. IV it is found that our predicted partial widths of $\Gamma[\Upsilon(3S) \to \chi_{bJ}(2P)\gamma]$ are in good agreement with the experimental data and the predictions in Refs. [11–16]. Combining our predicted partial widths with the measured width of $\Upsilon(3S)$, we estimate that

$$\mathcal{B}[\Upsilon(3S) \to \chi_{b0}(2P)\gamma] \simeq 5.5\%, \quad (46)$$
$$\mathcal{B}[\Upsilon(3S) \to \chi_{b1}(2P)\gamma] \simeq 12.8\%, \quad (47)$$
$$\mathcal{B}[\Upsilon(3S) \to \chi_{b2}(2P)\gamma] \simeq 15.6\%, \quad (48)$$

which are also in good agreement with the data from the PDG [8].

For the typical M1 transitions $\Upsilon(3S) \to \eta_b(1S, 2S)\gamma$, our predicted partial widths are listed in Tab. III. Our results are the same order of magnitude as the predictions from the recent nonrelativistic constituent quark model [13]. However, our prediction of the $\Gamma[\Upsilon(3S) \to \eta_b(1S)\gamma] \simeq 71$ eV is notably larger than the world average data 10 ± 2 eV [8]. To clarify this puzzle, more studies are needed.

2. $\eta_b(3S)$

The 3^1S_0 state, $\eta_b(3S)$, is still missing. The predicted mass splitting between 3^3S_1 and 3^1S_0 is about 17 MeV. Combining it with the measured mass of 3^3S_1, we predict that the mass of $\eta_b(3S)$ might be $M_{\eta_b(3S)} \simeq 10338$ MeV. Using this predicted mass, we study the E1 transitions $\eta_b(3S) \to h_b(1P, 2P)\gamma$ and M1 transitions $\eta_b(3S) \to \Upsilon(1S, 2S)\gamma$. Our results have been listed in Tabs. III and IV.

From Tab. IV, it is found that with the corrections of the spin-dependent potentials to the wave functions, our predicted partial widths for the E1 transitions $\eta_b(3S) \to h_b(1P, 2P)\gamma$ are about a factor 2 smaller than the previous screened potential

model predictions [11]. Furthermore, it should be mentioned that our predicted partial width ratio

$$\frac{\Gamma[\eta_b(3S)\to h_b(2P)\gamma]}{\Gamma[\eta_b(3S)\to h_b(1P)\gamma]} \simeq 6.1, \quad (49)$$

is notably different from the other model predictions [11–13, 16]. From Tab. III, it is found that our predicted partial widths for the M1 transitions $\eta_b(3S)\to\Upsilon(1S,2S)\gamma$ are compatible with the recent predictions in Refs. [12, 13], however, our predictions are about a factor 3 larger than the predictions with the relativistic quark model [16]. These radiative transitions should be further studied in theory.

G. Radiative transitions of $2D$ states

Until now, no $2D$ bottomonium states have been observed in experiments. In our calculations, their masses are adopted from our potential model predictions.

1. $\Upsilon_3(2D)$

The radiative transitions of $\Upsilon_3(2D)$ are dominated by the $\chi_{b2}(2P)\gamma$ channel, and the partial width decaying into the $\chi_{b2}(1P)\gamma$ channel is also sizeable. Taking the mass of $M_{\Upsilon_3(2D)}=10436$ MeV predicted by us, we calculate the partial widths of $\Gamma[\Upsilon_3(2D)\to\chi_{b2}(1P,2P)\gamma]$. The results compared with the other model predictions are listed in Tab. V, where we can see that our predictions are compatible with the other model predictions. In Ref. [12], the total width of $\Upsilon_3(2D)$ is predicted to be $\Gamma_{\rm tot}\simeq 25$ keV. With this predicted width, we further estimate the branching ratios:

$$\mathcal{B}[\Upsilon_3(2D)\to\chi_{b2}(1P)\gamma] \simeq 21\%, \quad (50)$$
$$\mathcal{B}[\Upsilon_3(2D)\to\chi_{b2}(2P)\gamma] \simeq 68\%. \quad (51)$$

To establish the $\Upsilon_3(2D)$ state, the $\chi_{b2}(1P,2P)\gamma$ channels are worth observing.

2. $\Upsilon_2(2D)$

The radiative transitions of $\Upsilon_2(2D)$ are dominated by the $\chi_{b1}(2P)\gamma$ channel, and the partial widths decaying into the $\chi_{b2}(2P)\gamma$, $\chi_{b1}(1P)\gamma$ and $\chi_{b2}(1P)\gamma$ channels are also sizeable. With the predicted mass $M_{\Upsilon_2(2D)}=10432$ MeV, we predict the partial widths for these radiative transitions. Our results compared with the other model predictions are listed in Tab. V. From the table, it is seen that the partial widths predicted by us are comparable with the other model predictions in magnitude [11–13, 16]. However, it should be mentioned that the predicted ratios from different models are very different. In Ref. [12], the total width of $\Upsilon_2(2D)$ is predicted to be $\Gamma_{\rm tot}\simeq 23$ keV. With this predicted total width, we further estimate that

$$\mathcal{B}[\Upsilon_2(2D)\to\chi_{b1}(2P)\gamma] \simeq 50\%, \quad (52)$$
$$\mathcal{B}[\Upsilon_2(2D)\to\chi_{b2}(2P)\gamma] \simeq 16\%, \quad (53)$$
$$\mathcal{B}[\Upsilon_2(2D)\to\chi_{b1}(1P)\gamma] \simeq 17\%, \quad (54)$$
$$\mathcal{B}[\Upsilon_2(2D)\to\chi_{b2}(1P)\gamma] \simeq 5\%. \quad (55)$$

Observation of the $\chi_{b1,2}(2P)\gamma$ and $\chi_{b1}(1P)\gamma$ channels may be crucial to establish the missing $\Upsilon_2(2D)$ state.

3. $\Upsilon_1(2D)$

The radiative transitions of $\Upsilon_1(2D)$ are dominated by the $\chi_{b0,1}(2P)\gamma$ channels, and the partial widths decaying into the $\chi_{b0,1,2}(1P)\gamma$ and $\chi_{b2}(2P)\gamma$ channels are also sizeable. Taking the mass of $M_{\Upsilon_1(2D)}=10425$ MeV, we calculate the partial decay widths. Our predicted partial widths for the transitions $\Upsilon_1(2D)\to\chi_{b0,1,2}(1P,2P)\gamma$ compared with the other model predictions are listed in Tab. V. From the table, it is found that most of our predictions are compatible with the other potential predictions in magnitude. In Ref. [12], the total width of $\Upsilon_1(2D)$ is predicted to be $\Gamma_{\rm tot}\simeq 38$ keV, with this input, we estimate the branching ratios for the dominant radiative transitions of $\Upsilon_1(2D)$, which are

$$\mathcal{B}[\Upsilon_1(2D)\to\chi_{b0}(2P)\gamma] \simeq 25\%, \quad (56)$$
$$\mathcal{B}[\Upsilon_1(2D)\to\chi_{b1}(2P)\gamma] \simeq 18\%, \quad (57)$$
$$\mathcal{B}[\Upsilon_1(2D)\to\chi_{b0}(1P)\gamma] \simeq 15\%, \quad (58)$$
$$\mathcal{B}[\Upsilon_1(2D)\to\chi_{b1}(1P)\gamma] \simeq 7\%. \quad (59)$$

There may be hope for observing the missing $\Upsilon_1(2D)$ state in the $\chi_{b0,1}(2P)\gamma$ and $\chi_{b0,1}(1P)\gamma$ channels.

4. $\eta_{b2}(2D)$

The main EM decay channels of $\eta_{b2}(2D)$ are $h_b(2P)\gamma$ and $h_b(1P)\gamma$. With the mass $M_{\eta_{b2}(2D)}=10432$ MeV predicted by us, the partial widths of the transitions $\eta_{b2}(2D)\to h_b(1P,2P)\gamma$ are calculated. The results compared with the other model predictions are listed in Tab. V. It is found that the predicted partial widths roughly agree with the potential model predictions [11–13]. Using the predicted total width of $\eta_{b2}(2D)$ ($\Gamma_{\rm tot}\simeq 25$ keV) from [12], we predict that

$$\mathcal{B}[\eta_{b2}(2D)\to h_b(1P)\gamma] \simeq 23\%, \quad (60)$$
$$\mathcal{B}[\eta_{b2}(2D)\to h_b(2P)\gamma] \simeq 62\%. \quad (61)$$

To determine the missing $\eta_{b2}(2D)$ state in experiments, its transitions into the $h_b(1P,2P)\gamma$ channels are worth observing.

H. Radiative transitions of $3P$ states

In the past several years, obvious progress has been achieved in the observations of the $3P$ states. In 2011, the ATLAS Collaboration first discovered the $\chi_b(3P)$ through its radiative transitions to $\Upsilon(1S,2S)$ with $\Upsilon(1S,2S)\to\mu^+\mu^-$ at the LHC [59]. Only a few months after that, the $\chi_b(3P)$ state was confirmed by the D0 Collaboration [60]. Recently, the LHCb Collaboration also carried out a precise measurement of the

$\chi_b(3P)$ state, identifying $\chi_b(3P)$ as the $\chi_{b1}(3P)$ state [61, 62]. The measured mass of $\chi_{b1}(3P)$ is $M_{\chi_{b1}(3P)} \simeq 10516$ MeV. In our calculations, the mass splittings are predicted to be $M_{\chi_{b2}(3P)} - M_{\chi_{b1}(3P)} \simeq 13$ MeV, $M_{\chi_{b1}(3P)} - M_{\chi_{b0}(3P)} \simeq 25$ MeV, and $M_{h_b(3P)} - M_{\chi_{b1}(3P)} \simeq 4$ MeV. Combining these predicted mass splittings with the measured mass of $\chi_{b1}(3P)$, we estimate the masses of $\chi_{b2}(3P)$, $\chi_{b0}(3P)$ and $h_b(3P)$, which are $M_{\chi_{b2}(3P)} \simeq 10529$ MeV, $M_{\chi_{b0}(3P)} \simeq 10491$ MeV, and $M_{h_b(3P)} \simeq 10520$ MeV, respectively.

1. $\chi_{b1}(3P)$

The $\Upsilon(1S, 2S, 3S)\gamma$ are the main EM decay channels of $\chi_{b1}(3P)$. From Tab. IV, it is seen that our predicted partial widths for these channels are close to the recent predictions with the nonrelativistic constituent quark model [13], and the predictions with the previous SNR potential models [11]. Furthermore, taking the total width of $\chi_{b1}(3P)$, $\Gamma_{\rm tot} \simeq 117$ keV, predicted in Ref. [12] as an input, we estimate that

$$\mathcal{B}[\chi_{b1}(3P) \to \Upsilon(1S)\gamma] \simeq 5.4\%, \quad (62)$$
$$\mathcal{B}[\chi_{b1}(3P) \to \Upsilon(2S)\gamma] \simeq 4.8\%, \quad (63)$$
$$\mathcal{B}[\chi_{b1}(3P) \to \Upsilon(3S)\gamma] \simeq 8.8\%. \quad (64)$$

These large branching ratios may explain why $\chi_b(3P)$ is discovered through its radiative transitions into $\Upsilon(1S, 2S)$.

Taking the masses of $2D$ waves calculated by us, we predict the partial widths for the transitions $\chi_{b1}(3P) \to \Upsilon_{1,2}(2D)\gamma$. Our results are listed in Tab. IV. From the table, it is found that our results are close to the potential model predictions [11, 12]. Similarly, with the predicted total width $\chi_{b1}(3P)$ from [12], we estimate that

$$\mathcal{B}[\chi_{b1}(3P) \to \Upsilon_1(2D)\gamma] \simeq 9.0 \times 10^{-3}, \quad (65)$$
$$\mathcal{B}[\chi_{b1}(3P) \to \Upsilon_2(2D)\gamma] \simeq 8.0 \times 10^{-3}. \quad (66)$$

The sizeable branching ratios of $\mathcal{B}[\chi_{b1}(3P) \to \Upsilon_{1,2}(2D)\gamma]$ indicate that one may discover the missing D-wave states $\Upsilon_1(2D)$ and $\Upsilon_2(2D)$ through the radiative transition chains $\chi_{b1}(3P) \to \Upsilon_{1,2}(2D)\gamma \to \chi_{b1}(1P, 2P)\gamma\gamma \to \Upsilon(1S, 2S)\gamma\gamma\gamma$. We further estimate the branching ratios for these decay chains. The results are listed in Tab. VII. It is found that the important chains involving $\Upsilon_1(2D)$ are $\chi_{b1}(3P) \to \Upsilon_1(2D)\gamma \to \chi_{b1}(2P, 1P)\gamma\gamma \to \Upsilon(1S, 2S)\gamma\gamma\gamma$ [$\mathcal{B} \sim O(10^{-4})$]. While the important chains involving $\Upsilon_2(2D)$ are $\chi_{b1}(3P) \to \Upsilon_2(2D)\gamma \to \chi_{b1}(2P)\gamma\gamma \to \Upsilon(2S)\gamma\gamma\gamma$ [$\mathcal{B} \simeq 4.6 \times 10^{-4}$], $\chi_{b1}(3P) \to \Upsilon_2(2D)\gamma \to \chi_{b1}(1P)\gamma\gamma \to \Upsilon(1S)\gamma\gamma\gamma$ [$\mathcal{B} \simeq 4.6 \times 10^{-4}$], and $\chi_{b1}(3P) \to \Upsilon_2(2D)\gamma \to \chi_{b1}(2P)\gamma\gamma \to \Upsilon(1S)\gamma\gamma\gamma$ [$\mathcal{B} \simeq 3.2 \times 10^{-4}$].

2. $\chi_{b2}(3P)$

With $M_{\chi_{b2}(3P)} = 10529$ MeV for the $\chi_{b2}(3P)$ state, we calculate its radiative decay properties. Our results are listed in Tab. IV. For comparison, the other model predictions are also listed in the same table. It is found that the radiative decay ratios of $\chi_{b2}(3P)$ into the $1D$-wave states are negligibly small, while the partial widths for the transitions $\chi_{b2}(3P) \to \Upsilon(1S, 2S, 3S)\gamma$ and $\chi_{b2}(3P) \to \Upsilon_3(2D)\gamma$ are sizeable. Most of our results are consistent with the other predictions. Taking the total width of $\chi_{b2}(3P)$, $\Gamma_{\rm tot} \simeq 247$ keV, predicted in Ref. [12] as an input, we estimate that

$$\mathcal{B}[\chi_{b2}(3P) \to \Upsilon(1S)\gamma] \simeq 3.3\%, \quad (67)$$
$$\mathcal{B}[\chi_{b2}(3P) \to \Upsilon(2S)\gamma] \simeq 2.7\%, \quad (68)$$
$$\mathcal{B}[\chi_{b2}(3P) \to \Upsilon(3S)\gamma] \simeq 4.4\%. \quad (69)$$

These fairly large branching ratios indicate the missing $\chi_{b2}(3P)$ state is most likely to be established via the radiative decays $\chi_{b2}(3P) \to \Upsilon(1S, 2S, 3S)\gamma$. Furthermore, we find that the branching ratio

$$\mathcal{B}[\chi_{b2}(3P) \to \Upsilon_3(2D)\gamma] \simeq 1.9\% \quad (70)$$

is sizeable. Thus, $\chi_{b2}(3P)$ might be a good source when looking for the missing $\Upsilon_3(2D)$. According to our analysis, the important radiative decay chains involving $\Upsilon_3(2D)$ are $\chi_{b2}(3P) \to \Upsilon_3(2D)\gamma \to \chi_{b2}(2P)\gamma\gamma \to \Upsilon(1S, 2S)\gamma\gamma\gamma$, and their combined branching ratios can reach up to $\mathcal{B} \simeq 1.3 \times 10^{-3}$.

3. $\chi_{b0}(3P)$

With the predicted mass $M_{\chi_{b0}(3P)} = 10491$ MeV for the $\chi_{b0}(3P)$ state, we calculate its radiative decay properties. Our results are listed in Tab. IV. It is found that the partial radiative decay widths of $\chi_{b0}(3P)$ into the S-wave states $\Upsilon(1S, 2S, 3S)$ are comparable to those of $\chi_{b1,2}(3P)$. In Ref. [12], the total width of $\chi_{b0}(3P)$ is predicted to be $\Gamma_{\rm tot} \simeq 2.5$ MeV, with which we estimate that

$$\mathcal{B}[\chi_{b0}(3P) \to \Upsilon(1S)\gamma] \simeq 7.5 \times 10^{-4}, \quad (71)$$
$$\mathcal{B}[\chi_{b0}(3P) \to \Upsilon(2S)\gamma] \simeq 1.0 \times 10^{-4}, \quad (72)$$
$$\mathcal{B}[\chi_{b0}(3P) \to \Upsilon(3S)\gamma] \simeq 3.2 \times 10^{-4}. \quad (73)$$

These branching ratios are about an order of magnitude smaller than those of $\mathcal{B}[\chi_{b1,2}(3P) \to \Upsilon(1S, 2S, 3S)\gamma]$, which may indicate that $\chi_{b0}(3P)$ is relatively difficult to observe in the $\Upsilon(1S, 2S, 3S)\gamma$ channels.

4. $h_b(3P)$

For the singlet $h_b(3P)$ state, with the predicted mass $M_{h_b(3P)} = 10520$ MeV, we calculate the radiative decay properties. Our results are listed in Tab. IV. The EM decays of $h_b(3P)$ are dominated by the $\eta_b(3S)\gamma$ channel, while the partial widths into the $\eta_b(1S, 2S)\gamma$ and $\eta_{b2}(2D)\gamma$ channels are sizeable as well. Our predicted partial decay widths into the S-wave states are the same order of those from various potential models [11–13] (see Tab. IV). Taking the predicted width of $h_b(3P)$, $\Gamma_{\rm tot} \simeq 83$ keV, from Ref. [12] as an input, we obtain

$$\mathcal{B}[h_b(3P) \to \eta_b(1S)\gamma] \simeq 12.9\%, \quad (74)$$
$$\mathcal{B}[h_b(3P) \to \eta_b(2S)\gamma] \simeq 9.2\%, \quad (75)$$
$$\mathcal{B}[h_b(3P) \to \eta_b(3S)\gamma] \simeq 17.0\%. \quad (76)$$

To look for the missing $h_b(3P)$ state, the transitions $h_b(3P) \to \eta_b(1S, 2S)\gamma$ are worth observing.

I. Radiative transitions of $4S$ states

$\Upsilon(4S)$ is established in experiments. Its mass and width are $M_{\Upsilon(4S)} \simeq 10579$ MeV and $\Gamma \simeq 20.5$ MeV, respectively. However, the $\eta_b(4S)$ is still missing. We predict their radiative properties. The results compared with the other predictions are listed in Tab. IV. From the table, it is found that obvious model dependencies exist in these predictions. Our calculations give relatively large decay rates for the $\Upsilon(4S) \to \chi_{bJ}(3P)\gamma$ transitions. Thus, the missing $\chi_{bJ}(3P)$ states might be produced by the radiative decay chains of $\Upsilon(4S) \to \chi_{bJ}(3P)\gamma \to \Upsilon(1S, 2S, 3S)\gamma\gamma$. Combining the predicted branching ratios of $\chi_{bJ}(3P) \to \Upsilon(1S, 2S, 3S)\gamma$ and $\Upsilon(4S) \to \chi_{bJ}(3P)\gamma$, we further estimate the combined branching ratios, which have been listed in Tab. VI. From the table, one can see that the most prominent two-photon decay chains are $\Upsilon(4S) \to \chi_{b1}(3P)\gamma \to \Upsilon(1S, 2S, 3S)\gamma\gamma$ [$\mathcal{B} \sim O(10^{-5})$], followed by $\Upsilon(4S) \to \chi_{b2}(3P)\gamma \to \Upsilon(1S, 2S, 3S)\gamma\gamma$ [$\mathcal{B} \sim O(10^{-6})$]. There are few chances for $\chi_{b0}(3P)$ to be observed in the radiative decay chains of $\Upsilon(4S)$.

IV. SUMMARY

In the nonrelativistic screened potential quark model framework, we study the bottomonium spectrum. The radial Schrödinger equation is solved with the three-point difference central method, where the spin-dependent potentials are dealt with non-perturbatively. In our calculations, the corrections of the spin-dependent interactions to the wave functions are successfully included as well. It is found that the corrections of spin-dependent interactions to the wave functions of the S-wave and $^3P_{0,1}$ states are notably big. The bottomonium spectrum predicted within our approach is in a global agreement with the experimental data.

Moreover, using the obtained wave functions we study the EM transitions of nS ($n \leq 4$), nP ($n \leq 3$), and nD ($n \leq 2$) bottomonium states with a nonrelativistic EM transition operator widely applied to meson photoproduction reactions, in which the effects of binding potential between quarks are considered, and the possible higher EM multipole contributions are included. It is found that (i) except for some M1 transitions, our predictions for the EM transitions are in good agreement with the experimental data. (ii) The corrections of the spin-dependent interactions are important to understand some EM transitions. For example, the EM transitions of $\Upsilon(3S) \to \chi_{b1,2}(1P)\gamma$, which were not well understood in previous studies, can be reasonably explained in the present work by considering the corrections of the spin-dependent interactions to the wave functions. (iii) Strong model dependencies exist in various model predictions of some transition widths, especially for the partial width ratios. To test the various model predictions more observations are expected to be carried out in forthcoming experiments.

Additionally, we discuss the observations of the missing bottomonium states by using radiative transitions. (i) We suggest our experimental colleagues observe the three-photon decay chains $\chi_{b2}(2P) \to \Upsilon_3(1D)\gamma \to \chi_{b2}(1P)\gamma\gamma \to \Upsilon(1S)\gamma\gamma\gamma$ [$\mathcal{B} \sim O(10^{-3})$] and $h_b(2P) \to \eta_{b2}(1D)\gamma \to h_b(1P)\gamma\gamma \to \eta_b\gamma\gamma\gamma$ ($\mathcal{B} \simeq 1.4\%$), where the missing $\Upsilon_3(1D)$ and $\eta_{b2}(1D)$ states are most likely to be observed. (ii) We also suggest our experimental colleagues observe the following three-photon decay chains: $\chi_{b1}(3P) \to \Upsilon_1(2D)\gamma \to \chi_{b1}(2P, 1P)\gamma\gamma \to \Upsilon(1S, 2S)\gamma\gamma\gamma$ [$\mathcal{B} \sim O(10^{-4})$], $\chi_{b1}(3P) \to \Upsilon_2(2D)\gamma \to \chi_{b1}(2P)\gamma\gamma \to \Upsilon(2S)\gamma\gamma\gamma$ [$\mathcal{B} \simeq 4.6 \times 10^{-4}$], $\chi_{b1}(3P) \to \Upsilon_2(2D)\gamma \to \chi_{b1}(1P)\gamma\gamma \to \Upsilon(1S)\gamma\gamma\gamma$ [$\mathcal{B} \simeq 4.6 \times 10^{-4}$], and $\chi_{b1}(3P) \to \Upsilon_2(2D)\gamma \to \chi_{b1}(2P)\gamma\gamma \to \Upsilon(1S)\gamma\gamma\gamma$ [$\mathcal{B} \simeq 3.2 \times 10^{-4}$], where the missing $\Upsilon_1(2D)$ and $\Upsilon_2(2D)$ states might have chances to be observed. (iii) The missing $\chi_{bJ}(3P)$ states might be produced via the radiative transitions of $\Upsilon(4S)$. The most prominent decay chains are $\Upsilon(4S) \to \chi_{b1}(3P)\gamma \to \Upsilon(1S, 2S, 3S)\gamma\gamma$ [$\mathcal{B} \sim O(10^{-5})$], followed by $\Upsilon(4S) \to \chi_{b2}(3P)\gamma \to \Upsilon(1S, 2S, 3S)\gamma\gamma$ [$\mathcal{B} \sim O(10^{-6})$].

The LHC and Belle experiments have demonstrated the ability to observe and measure the properties of bottomonium mesons. In the near future, more missing bottomonium states are to be discovered and more decay channels will be measured in experiments. We expect that our theoretical predictions in this paper will be helpful for experimental exploration of the bottomonium mesons.

Acknowledgements

This work is supported, in part, by the National Natural Science Foundation of China (Grants No. 11075051 and No. 11375061), and the Hunan Provincial Natural Science Foundation (Grant No. 13JJ1018).

Appendix

The method for solving Eq.(11) is outlined as follows. Equation (11) can be rewritten as

$$\frac{d^2u(r)}{dr^2} = T(r)u(r), \tag{77}$$

with $T(r) = -2\mu_R\left[E - V_{b\bar{b}}(r) - \frac{L(L+1)}{2\mu_R r^2}\right]$. According to the Gowell central difference method, we have [53]

$$u(r_{i+1}) = \frac{[2 + \frac{5}{6}h^2T(r_i)]u(r_i) - [1 - \frac{1}{12}h^2T(r_{i-1})]u(r_{i-1})}{1 - \frac{1}{12}h^2T(r_{i+1})}, \tag{78}$$

with $r_i = ih$ ($i = 0, 1, 2 \cdot \cdot\cdot$). The starting conditions of the above equation are

$$u(0) = 0, \quad u(h) = h^{L+1},$$
$$T(0)u(0) = \lim_{r\to 0}\frac{L(L+1)}{r^2}r^{L+1} = 2\delta_{L1}. \tag{79}$$

Thus, for a given binding energy E, in terms of Eq.(78), the radial wave function $u(r)$ can be calculated from the center ($r = 0$) towards the outside ($r \to \infty$) point by point.

Finally, to determine the binding energy E, we adopt the following method. As we know if E_0 is a trial value near the eigenvalue of the binding energy E, the asymptotic form of the numerical solution of the radial wave function $u(r, E_0)$ at large r is given by the linear combination of the regular solution $g(E_0)e^{-k_0 r}$ and irregular solution $f(E_0)e^{+k_0 r}$ with $k_0^2 = 2\mu E_0$. Thus, we can take the radial wave function $u(r, E_0)$ at large r as [53]

$$u(r, E_0) = f(E_0)e^{+k_0 r}, \tag{80}$$

Similarly, for another trial value E_1, we have

$$u(r, E_1) = f(E_1)e^{+k_1 r}, \tag{81}$$

with $k_1^2 = 2\mu E_1$. If $f(E)$ is an analytic function, we can expand $f(E_1)$ as

$$f(E_1) = f(E_0) + f'(E_0)(E_1 - E_0) + \cdots. \tag{82}$$

If $|E_1 - E_0|$ is small enough, we can only keep the first two terms. Then, we have

$$f'(E_0) = \frac{f(E_1) - f(E_0)}{E_1 - E_0} = \frac{u(r, E_1)e^{-k_1 r} - u(r, E_0)e^{-k_0 r}}{E_1 - E_0}. \tag{83}$$

Note that, if E_1 is just the eigenvalue of the binding energy E, $f(E_1)$ should be zero. Thus, from Eq.(82) we have

$$E = E_0 - f(E_0)/f'(E_0) \tag{84}$$

In the numerical calculations, the recurrence method is used to calculate the eigenvalue E. Letting $E_1 \to E_0$, $u(r, E_1) \to u(r, E_0)$ and $E \to E_1$, then we calculate new $u(r, E_1)$ and new E with Eqs.(78) and (79). The recurrence is stopped when $|E - E_0| \leq \epsilon$, where ϵ stands for the accuracy that we need.

[1] S. Godfrey and N. Isgur, Mesons in a Relativized Quark Model with Chromodynamics, Phys. Rev. D **32**, 189 (1985).

[2] E. Eichten, K. Gottfried, T. Kinoshita, K. D. Lane and T. M. Yan, Charmonium: The Model, Phys. Rev. D **17**, 3090 (1978) Erratum: [Phys. Rev. D **21**, 313 (1980)].

[3] A. Garmash, Bottomonium Studies at Belle, EPJ Web Conf. **96**, 01014 (2015).

[4] E. Eichten, S. Godfrey, H. Mahlke and J. L. Rosner, Quarkonia and their transitions, Rev. Mod. Phys. **80**, 1161 (2008).

[5] N. Brambilla *et al.* [Quarkonium Working Group Collaboration], Heavy quarkonium physics, hep-ph/0412158.

[6] N. Brambilla *et al.*, Heavy quarkonium: progress, puzzles, and opportunities, Eur. Phys. J. C **71**, 1534 (2011).

[7] A. J. Bevan *et al.* [BaBar and Belle Collaborations], The Physics of the *B* Factories, Eur. Phys. J. C **74**, 3026 (2014).

[8] K. A. Olive *et al.* [Particle Data Group Collaboration], Review of Particle Physics, Chin. Phys. C **38**, 090001 (2014).

[9] S. N. Gupta, S. F. Radford and W. W. Repko, $b\bar{b}$ Spectroscopy, Phys. Rev. D **30**, 2424 (1984).

[10] W. Kwong and J. L. Rosner, *D* Wave Quarkonium Levels of the Υ Family, Phys. Rev. D **38**, 279 (1988).

[11] B. Q. Li and K. T. Chao, Bottomonium Spectrum with Screened Potential, Commun. Theor. Phys. **52**, 653 (2009).

[12] S. Godfrey and K. Moats, Bottomonium Mesons and Strategies for their Observation, Phys. Rev. D **92**, 054034 (2015).

[13] J. Segovia, P. G. Ortega, D. R. Entem and F. Fernández, Bottomonium spectrum revisited, Phys. Rev. D **93**, 074027 (2016).

[14] A. Barducci, R. Giachetti and E. Sorace, Relativistic two-body calculation of $b\bar{b}$-mesons radiative decays, arXiv:1604.08043 [hep-ph].

[15] Wei-Zhao Tian, Lu Cao, You-Chang Yang and Hong Chen, Bottomonium states versus recent experimental observations in the QCD-inspired potential model, Chin. Phys. C **37**, 083101 (2013).

[16] D. Ebert, R. N. Faustov and V. O. Galkin, Properties of heavy quarkonia and B_c mesons in the relativistic quark model, Phys. Rev. D **67**, 014027 (2003).

[17] N. Akbar, M. A. Sultan, B. Masud and F. A. Sultan, Higher Hybrid Bottomonia in an Extended Potential Model, arXiv:1511.03632 [hep-ph].

[18] C. Hughes, R. J. Dowdall, C. T. H. Davies, R. R. Horgan, G. von Hippel and M. Wingate, Hindered M1 Radiative Decay of $\Upsilon(2S)$ from Lattice NRQCD, Phys. Rev. D **92**, 094501 (2015).

[19] R. Lewis and R. M. Woloshyn, Excited Upsilon Radiative Decays, Phys. Rev. D **84**, 094501 (2011).

[20] D. Becirevi, M. Kruse and F. Sanfilippo, Lattice QCD estimate of the $\eta_c(2S) \to J/\psi\gamma$ decay rate, JHEP **1505**, 014 (2015).

[21] M. Baker, A. A. Penin, D. Seidel and N. Zerf, Bottomonium Hyperfine Splitting on the Lattice and in the Continuum, Phys. Rev. D **92**, 054502 (2015).

[22] F. De Fazio, Radiative transitions of heavy quarkonium states, Phys. Rev. D **79**, 054015 (2009) Erratum: [Phys. Rev. D **83**, 099901 (2011)].

[23] N. Brambilla, Y. Jia and A. Vairo, Model-independent study of magnetic dipole transitions in quarkonium, Phys. Rev. D **73**, 054005 (2006).

[24] N. Brambilla, P. Pietrulewicz and A. Vairo, Model-independent Study of Electric Dipole Transitions in Quarkonium, Phys. Rev. D **85**, 094005 (2012).

[25] A. Pineda and J. Segovia, Improved determination of heavy quarkonium magnetic dipole transitions in potential nonrelativistic QCD, Phys. Rev. D **87**, 074024 (2013).

[26] J. Ferretti and E. Santopinto, Higher mass bottomonia, Phys. Rev. D **90**, 094022 (2014).

[27] J. Ferretti, G. Galat and E. Santopinto, Quark structure of the $X(3872)$ and $\chi_b(3P)$ resonances, Phys. Rev. D **90**, 054010 (2014).

[28] Y. Lu, M. N. Anwar and B. S. Zou, Coupled-Channel Effects for the Bottomonium with Realistic Wave Functions, Phys. Rev. D **94**, 034021 (2016).

[29] H. M. Choi, Decay constants and radiative decays of heavy mesons in light-front quark model, Phys. Rev. D **75**, 073016 (2007).

[30] H. W. Ke, X. Q. Li, Z. T. Wei and X. Liu, Re-Study on the wave functions of $\Upsilon(nS)$ states in LFQM and the radiative decays of $\Upsilon(nS) \to \eta_b\gamma$, Phys. Rev. D **82**, 034023 (2010).

[31] H. W. Ke, X. Q. Li and X. Liu, Study on the Radiative Decays

of $\Upsilon(nS) \to \eta_b\gamma$, arXiv:1002.1187 [hep-ph].
[32] H. W. Ke, X. Q. Li and Y. L. Shi, The radiative decays of 0^{++} and 1^{+-} heavy mesons, Phys. Rev. D **87**, 054022 (2013).
[33] B. Q. Li and K. T. Chao, Higher Charmonia and X,Y,Z states with Screened Potential, Phys. Rev. D **79**, 094004 (2009).
[34] K.T. Chao and J.H. Liu, in Proceedings of the Workshop on Weak Interactions and CP Violation, Beijing, August 22-26, 1989, edited by T. Huang and D.D. Wu, World Scientific (Singapore, 1990) p.109-p.117.
[35] Y. B. Ding, K. T. Chao and D. H. Qin, Screened $Q\bar{Q}$ potential and spectrum of heavy quarkonium, Chin. Phys. Lett.**10**, 460 (1993).
[36] E. Laermann, F. Langhammer, I. Schmitt and P. M. Zerwas, The Interquark Potential: SU(2) Color Gauge Theory With Fermions, Phys. Lett. B **173**, 437 (1986).
[37] K. D. Born, E. Laermann, N. Pirch, T. F. Walsh and P. M. Zerwas, Hadron Properties in Lattice QCD With Dynamical Fermions, Phys. Rev. D **40**, 1653 (1989).
[38] W. J. Deng, L. Y. Xiao, L. C. Gui and X. H. Zhong, Radiative transitions of charmonium states, arXiv:1510.08269 [hep-ph].
[39] Zhenping Li, Threshold pion photoproduction of nucleons in the chiral quark model, Phys. Rev. D **50**, 5639 (1994).
[40] Zhenping Li, The Kaon photoproduction of nucleons in the chiral quark model, Phys. Rev. C **52**, 1648 (1995).
[41] Zhenping Li, H. X. Ye and M. H. Lu, An unified approach to pseudoscalar meson photoproductions off nucleons in the quark model, Phys. Rev. C **56**, 1099 (1997).
[42] Q. Zhao, Eta-prime photoproduction near threshold, Phys. Rev. C **63**, 035205 (2001).
[43] B. Saghai and Zhenping Li, Quark model study of the eta photoproduction: Evidence for a new S_{11} resonance?, Eur. Phys. J. A **11**, 217 (2001).
[44] Q. Zhao, J. S. Al-Khalili, Z. P. Li and R. L. Workman, Pion photoproduction on the nucleon in the quark model, Phys. Rev. C **65**, 065204 (2002).
[45] J. He, B. Saghai and Z. Li, Study of η photoproduction on the proton in a chiral constituent quark approach via one-gluon-exchange model, Phys. Rev. C **78**, 035204 (2008).
[46] J. He and B. Saghai, Combined study of $\gamma p \to \eta p$ and $\pi^- p \to \eta n$ in a chiral constituent quark approach, Phys. Rev. C **80**, 015207 (2009).
[47] J. He and B. Saghai, η production off the proton in a Regge-plus-chiral quark approach, Phys. Rev. C **82**, 035206 (2010).
[48] X. H. Zhong and Q. Zhao, η photoproduction on the quasi-free nucleons in the chiral quark model, Phys. Rev. C **84**, 045207 (2011).
[49] X. H. Zhong and Q. Zhao, η' photoproduction on the nucleons in the quark model, Phys. Rev. C **84**, 065204 (2011).
[50] L. Y. Xiao, X. Cao and X. H. Zhong, Neutral pion photoproduction on the nucleon in a chiral quark model, Phys. Rev. C **92**, 035202 (2015).
[51] T. Barnes, S. Godfrey and E. S. Swanson, Higher charmonia, Phys. Rev. D **72**, 054026 (2005).
[52] D. Flamm and F. Schöber, Itroduction to the quark model of elementary particle, Volume 1: Quantum numbers, gauge theory and hadron spectroscopy, Gordon and Breach science publishers (1982).
[53] Chong-Hai Cai and Lei Li, Radial equation of bound state and binding energies of Ξ^- hypernuclei, High Energy Physics and Nuclear Physics **27**, 1005 (2003).
[54] A. Abdesselam *et al.*, Study of $\chi_{bJ}(1P)$ Properties in the Radiative $\Upsilon(2S)$ Decays, arXiv:1606.01276 [hep-ex].
[55] P. del Amo Sanchez *et al.* [BaBar Collaboration], Observation of the $\Upsilon(1^3D_J)$ Bottomonium State through Decays to $\pi^+\pi^-\Upsilon(1S)$, Phys. Rev. D **82**, 111102 (2010).
[56] C. Cawlfield *et al.* [CLEO Collaboration], Experimental study of $\chi_b(2P) \to \pi\pi\chi_b(1P)$, Phys. Rev. D **73**, 012003 (2006).
[57] R. Mizuk *et al.* [Belle Collaboration], Evidence for the $\eta_b(2S)$ and observation of $h_b(1P) \to \eta_b(1S)\gamma$ and $h_b(2P) \to \eta_b(1S)\gamma$, Phys. Rev. Lett. **109**, 232002 (2012).
[58] A. M. Badalian and B. L. G. Bakker, Dominant spin-orbit effects in radiative decays $\Upsilon(3S) \to \gamma\chi_{bJ}(1P)$), Phys. Rev. D **86**, 074001 (2012).
[59] G. Aad *et al.* [ATLAS Collaboration], Observation of a new χ_b state in radiative transitions to $\Upsilon(1S)$ and $\Upsilon(2S)$ at ATLAS, Phys. Rev. Lett. **108**, 152001 (2012).
[60] V. M. Abazov *et al.* [D0 Collaboration], Observation of a narrow mass state decaying into $\Upsilon(1S)\gamma$ in $p\bar{p}$ collisions at $\sqrt{s}$ = 1.96 TeV, Phys. Rev. D **86**, 031103 (2012).
[61] R. Aaij *et al.* [LHCb Collaboration], Measurement of the $\chi_b(3P)$ mass and of the relative rate of $\chi_{b1}(1P)$ and $\chi_{b2}(1P)$ production, JHEP **1410**, 88 (2014).
[62] R. Aaij *et al.* [LHCb Collaboration], Study of χ_b meson production in pp collisions at $\sqrt{s}$ = 7 and 8 TeV and observation of the decay $\chi_b(3P) \to \Upsilon(3S)\gamma$, Eur. Phys. J. C **74**, 3092 (2014).

TABLE IV: Partial widths of the radiative transitions for the nS- and nP-wave ($n = 2, 3$) bottomonium states. For comparison, the measured values from the PDG [8], the predictions from the relativistic quark model [16], relativized quark model (GI model) [12], nonrelativistic constituent quark model (NR model) [13], and the previous screened potential model (SNR model) [11] are listed in the table as well. SNR_0 and SNR_1 stand for the results calculated by the zeroth-order wave functions and the first-order relativistically corrected wave functions with the screened potential model [11], respectively.

Initial	Final	E_γ (MeV)				Γ_{E1} (keV)					Γ_{EM} (keV)	
state	state	Ref.[16]	$SNR_{0,1}$[11]	GI [12]	ours	Ref.[16]	SNR_0[11]	SNR_1[11]	GI [12]	NR [13]	Ours	PDG [8]
$\Upsilon(2^3S_1)$	$\chi_{b2}(1^3P_2)$	109	110	110	110	2.46	2.62	2.46	1.88	2.08	2.62	2.29 ± 0.20
	$\chi_{b1}(1^3P_1)$	130	130	129	129	2.45	2.54	2.08	1.63	1.84	2.17	2.21 ± 0.19
	$\chi_{b0}(1^3P_0)$	162	163	163	163	1.62	1.67	1.11	0.91	1.09	1.09	1.22 ± 0.11
$\eta_b(2^1S_0)$	$h_b(1^1P_1)$	98	83	99	99	3.09	6.10	5.57	2.48	2.85	3.41	
$\Upsilon(3^3S_1)$	$\chi_{b2}(2^3P_2)$	86	86	86	86	2.67	3.23	3.04	2.30	2.56	3.16	2.66 ± 0.27
	$\chi_{b1}(2^3P_1)$	100	99	100	100	2.41	2.96	2.44	1.91	2.13	2.61	2.56 ± 0.26
	$\chi_{b0}(2^3P_0)$	123	122	121	121	1.49	1.83	1.23	1.03	1.21	1.21	1.20 ± 0.12
	$\chi_{b2}(1^3P_2)$	433	434	434	434	0.097	0.25	1.26	0.45	0.083	0.14	0.20 ± 0.03
	$\chi_{b1}(1^3P_1)$	453	452	452	452	0.067	0.17	0.14	0.05	0.16	0.0005	0.018 ± 0.010
	$\chi_{b0}(1^3P_0)$	484	484	484	484	0.027	0.07	0.05	0.01	0.15	0.097	0.055 ± 0.010
$\eta_b(3^1S_0)$	$h_b(2^1P_1)$	73	74	77	78	2.78	11.0	10.1	2.96	2.60	4.25	
	$h_b(1^1P_1)$	427	418	429	429	0.348	1.24	5.68	1.30	0.0084	0.67	
$\chi_{b2}(2^3P_2)$	$\Upsilon(1^3D_3)$	108	113	97	101	2.35	3.33	3.13	1.5	2.06	2.51	
	$\Upsilon(1^3D_2)$	111	117	104	104	0.449	0.66	0.58	0.3	0.35	0.42	
	$\Upsilon(1^3D_1)$	117	123	113	111	0.035	0.05	0.04	0.03	0.021	0.026	
	$\Upsilon(2^3S_1)$	243	243	243	243	16.7	18.8	14.2	14.3	17.50	15.3	15.1 ± 5.6
	$\Upsilon(1^3S_1)$	776	777	777	777	8.02	13.0	12.5	8.4	11.38	12.5	9.8 ± 2.3
$\chi_{b1}(2^3P_1)$	$\Upsilon(1^3D_2)$	98	104	91	91	1.56	2.31	2.26	1.2	1.26	0.50	
	$\Upsilon(1^3D_1)$	104	110	100	98	0.615	0.92	0.84	0.5	0.41	0.56	
	$\Upsilon(2^3S_1)$	230	230	229	229	14.7	15.9	13.8	13.3	15.89	15.3	19.4 ± 5.0
	$\Upsilon(1^3S_1)$	764	764	764	764	7.49	12.4	8.56	5.5	9.13	10.8	8.9 ± 2.2
$\chi_{b0}(2^3P_0)$	$\Upsilon(1^3D_1)$	81	87	78	78	1.17	1.83	1.85	1.0	0.74	1.77	
	$\Upsilon(2^3S_1)$	207	207	208	208	11.0	11.7	11.6	10.9	12.80	14.4	
	$\Upsilon(1^3S_1)$	743	743	744	744	6.79	11.4	4.50	2.5	5.44	5.54	
$h_b(2^1P_1)$	$\eta_{b2}(1^1D_2)$	102	104	95	95	2.43	7.74	7.42	1.7	5.36	2.24	
	$\eta_b'(2^1S_0)$	262	266	258	258	21.4	24.7	15.3	14.1	17.60	16.2	
	$\eta_b(1^1S_0)$	820	831	826	826	9.36	15.9	18.0	13.0	14.90	16.1	
$\chi_{b2}(3^3P_2)$	$\Upsilon(2^3D_3)$		97	73	93		5.05	4.69	1.5	4.16	4.60	
	$\Upsilon(2^3D_2)$		101	79	97		1.02	0.89	0.32	0.79	0.78	
	$\Upsilon(2^3D_1)$		107	87	103		0.08	0.07	0.027	0.18	0.049	
	$\Upsilon(1^3D_3)$		377	350	365		0	0.05	0.046	0.21	0.12	
	$\Upsilon(1^3D_2)$				358					0.044	0.068	
	$\Upsilon(1^3D_1)$				366					0.0034	0.047	
	$\Upsilon(3^3S_1)$		183	172	173		15.6	11.1	9.3	10.38	10.8	
	$\Upsilon(2^3S_1)$		504	493	494		6.00	6.89	4.5	5.62	6.72	
	$\Upsilon(1^3S_1)$		1024	1014	1014		7.09	6.76	2.8	5.65	8.17	
$\chi_{b1}(3^3P_1)$	$\Upsilon(2^3D_2)$		86	67	84		3.10	2.98	1.1	3.34	0.94	
	$\Upsilon(2^3D_1)$		92	75	90		1.26	1.13	0.47	1.26	1.07	
	$\Upsilon(1^3D_2)$		366	346	346		0	0.09	0.08	0.11	0.015	
	$\Upsilon(1^3D_1)$		372	355	355		0	0.00	0.007	0.048	0.010	
	$\Upsilon(3^3S_1)$		167	160	160		12.0	9.97	8.4	9.62	10.3	
	$\Upsilon(2^3S_1)$		489	481	481		5.48	5.39	3.1	4.58	5.63	
	$\Upsilon(1^3S_1)$		1010	1003	1003		6.80	3.39	1.3	4.17	6.41	
$\chi_{b0}(3^3P_0)$	$\Upsilon(2^3D_1)$			59	68				1.0	3.50	2.20	
	$\Upsilon(1^3D_1)$		351	339	341		0	0.17	0.20	0.036	0.15	
	$\Upsilon(3^3S_1)$		146	144	135		7.88	7.67	6.9	8.50	7.95	
	$\Upsilon(2^3S_1)$		468	466	458		4.80	3.67	1.7	2.99	2.55	
	$\Upsilon(1^3S_1)$		990	988	980		6.41	0.86	0.3	1.99	1.87	
$h_b(3^1P_1)$	$\eta_{b2}(2^1D_2)$			69	88				1.6	4.72	4.21	
	$\eta_{b2}(1^1D_2)$		370	348	360		0	0.24	0.081	0.35	0.17	
	$\eta_b(3^1S_0)$		196	180	194		19.2	11.6	8.9	12.27	14.1	
	$\eta_b(2^1S_0)$		528	507	508		6.89	10.3	8.2	6.86	7.63	

TABLE V: Partial widths of the radiative transitions for the $1P$-, $1D$- and $2D$-wave bottomonium states. For comparison, the predictions from the relativistic quark model [16], relativized quark model (GI model) [12], nonrelativistic constituent quark model (NR model) [13], and previous screened potential model (SNR model) [11] are listed in the table as well. SNR_0 and SNR_1 stand for the results calculated by the zeroth-order wave functions and the first-order relativistically corrected wave functions with the screened potential model [11], respectively.

Initial meson	Final meson	E_γ (MeV)				Γ_{E1} (keV)					Γ_{EM} (keV)
state	state	Ref.[16]	$\mathrm{SNR}_{0,1}$[11]	GI [12]	ours	Ref.[16]	SNR_0[11]	SNR_1[11]	GI [12]	NR [13]	Ours
$\chi_{b2}(1^3P_2)$	$\Upsilon(1^3S_1)$	442	442	442	442	40.2	38.2	32.6	32.8	39.15	31.8
$\chi_{b1}(1^3P_1)$		422	423	424	424	36.6	33.6	30.0	29.5	35.66	31.9
$\chi_{b0}(1^3P_0)$		391	391	391	391	29.9	26.6	24.3	23.8	28.07	27.5
$h_b(1^1P_1)$	$\eta_b(1^1S_0)$	480	501	488	488	52.6	55.8	36.3	35.7	43.66	35.8
$\Upsilon(1^3D_3)$	$\chi_{b2}(1^3P_2)$	244	240	257	253	24.6	26.4	24.5	24.3	24.74	32.1
	$\chi_{b1}(1^3P_1)$				271					0	1.1×10^{-2}
	$\chi_{b0}(1^3P_0)$				304					0	9.2×10^{-5}
$\Upsilon(1^3D_2)$	$\chi_{b2}(1^3P_2)$	241	236	249	249	6.35	6.29	5.87	5.6	6.23	7.23
	$\chi_{b1}(1^3P_1)$	262	255	267	267	23.3	23.8	19.8	19.2	21.95	21.8
	$\chi_{b0}(1^3P_0)$				300					0	0.83×10^{-2}
$\Upsilon(1^3D_1)$	$\chi_{b2}(1^3P_2)$	235	230	240	242	0.69	0.65	0.61	0.56	0.65	1.02
	$\chi_{b1}(1^3P_1)$	256	249	259	261	12.7	12.3	10.3	9.7	12.29	13.3
	$\chi_{b0}(1^3P_0)$	280	282	292	294	23.4	23.6	16.7	16.5	20.98	19.8
$\eta_{b2}(1^1D_2)$	$h_b(1^1P_1)$	254	246	263	262	28.4	42.3	36.5	24.9	17.23	30.3
$\Upsilon(2^3D_3)$	$\chi_{b2}(1^3P_2)$		517	529	511		4.01	3.73	2.6	3.80	5.22
	$\chi_{b1}(1^3P_1)$				535					0	0.16
	$\chi_{b0}(1^3P_0)$				567					0	0.08
	$\chi_{b2}(2^3P_2)$		172	184	166		18.0	15.9	16.4	10.70	17.0
	$\chi_{b1}(2^3P_1)$				185					0	0.34×10^{-2}
	$\chi_{b0}(2^3P_0)$				207					0	0.66×10^{-3}
$\Upsilon(2^3D_2)$	$\chi_{b2}(1^3P_2)$		513	523	507		0.98	0.68	0.4	0.80	1.11
	$\chi_{b1}(1^3P_1)$		531	541	525		3.26	4.46	2.6	3.43	4.00
	$\chi_{b0}(1^3P_0)$				555					0	0.89×10^{-2}
	$\chi_{b2}(2^3P_2)$		168	178	162		4.17	3.82	3.8	2.55	3.75
	$\chi_{b1}(2^3P_1)$		181	192	175		15.7	12.1	12.7	9.10	11.4
	$\chi_{b0}(2^3P_0)$				197					0	1.7×10^{-3}
$\Upsilon(2^3D_1)$	$\chi_{b2}(1^3P_2)$		507	516	500		0.11	0.05	0.9	0.061	0.44
	$\chi_{b1}(1^3P_1)$		525	534	518		1.76	1.87	2.9	1.58	2.17
	$\chi_{b0}(1^3P_0)$		557	566	551		2.79	6.20	1.6	3.52	5.56
	$\chi_{b2}(2^3P_2)$		162	171	155		0.42	0.39	0.4	0.24	0.47
	$\chi_{b1}(2^3P_1)$		175	184	167		7.87	6.35	6.5	4.84	6.74
	$\chi_{b0}(2^3P_0)$		198	206	190		15.1	9.49	10.6	8.35	9.58
$\eta_{b2}(2^1D_2)$	$h_b(1^1P_1)$		522	536	519		6.19	7.30	3.0	4.15	5.66
	$h_b(2^1P_1)$		181	188	171		31.3	25.4	16.5	11.66	15.6

TABLE VI: Partial widths of the radiative transitions for the higher $4S$ states. For comparison, the predictions from the relativized quark model (GI model) [12], nonrelativistic constituent quark model (NR model) [13], and the previous screened potential model (SNR model) [11] are listed in the table as well. SNR_0 and SNR_1 stand for the results calculated by the zeroth-order wave functions and the first-order relativistically corrected wave functions with the screened potential model [11], respectively.

Initial	Final	E_γ (MeV)			Γ_{E1} (keV)			Γ_{EM} (keV)
state	state	SNR [11]	GI [12]	Ours	$\mathrm{SNR}_0/\mathrm{SNR}_1$ [11]	NR [13]	GI [12]	Ours
$\Upsilon(4S)$	$\chi_{b2}(1P)$	646		646	0.14/0.56	0.012		0.66
	$\chi_{b1}(1P)$	664		664	0.10/0.20	0.047		0.017
	$\chi_{b0}(1P)$	695		695	0.04/0.001	0.059		0.14
	$\chi_{b2}(2P)$	306		305	0.14/0.56	0.11		0.34
	$\chi_{b1}(2P)$	319		319	0.09/0.001	0.18		0.024
	$\chi_{b0}(2P)$	341		340	0.04/0.21	0.17		0.44
	$\chi_{b2}(3P)$	40	51	50	0.55/0.52	1.45	0.82	4.4
	$\chi_{b1}(3P)$	55	63	64	0.91/0.74	1.17	0.84	4.9
	$\chi_{b0}(3P)$	77	79	89	0.82/0.54	0.61	0.48	3.4
$\eta_b(4S)$	$h_c(1P)$	669		663	0.90/5.64			1.98
	$h_c(2P)$	334		319	0.95/2.16			1.56
	$h_c(3P)$	67	48	65	1.24/5.68		1.24	17.4

TABLE VII: Three-photon decay chains of 3^3P_2. The combined branching fractions of the chain are defined by $\mathcal{B} = \mathcal{B}_1 \times \mathcal{B}_2 \times \mathcal{B}_3$ with $\mathcal{B}_1 = \mathcal{B}[3^3P_1 \to 2^3D_J\gamma]$, $\mathcal{B}_2 = \mathcal{B}[2^3D_J \to m^3P_J\gamma]$, and $\mathcal{B}_3 = \mathcal{B}[m^3P_J \to \Upsilon(1S, 2S)\gamma]$.

Decay chain	$\mathcal{B}_1$	$\mathcal{B}_2$	$\mathcal{B}_3$	$\mathcal{B}$
$3^3P_1 \to 2^3D_1 \to 2^3P_0 \to \Upsilon(2S)$	9.0×10^{-3}	25%	5.8×10^{-3}	1.3×10^{-5}
$3^3P_1 \to 2^3D_1 \to 2^3P_1 \to \Upsilon(2S)$	9.0×10^{-3}	18%	11.5%	1.9×10^{-4}
$3^3P_1 \to 2^3D_1 \to 2^3P_0 \to \Upsilon(1S)$	9.0×10^{-3}	25%	2.2×10^{-3}	5.0×10^{-6}
$3^3P_1 \to 2^3D_1 \to 2^3P_1 \to \Upsilon(1S)$	9.0×10^{-3}	18%	8.1%	1.3×10^{-4}
$3^3P_1 \to 2^3D_1 \to 1^3P_0 \to \Upsilon(1S)$	9.0×10^{-3}	15%	1.76%	2.4×10^{-5}
$3^3P_1 \to 2^3D_1 \to 1^3P_1 \to \Upsilon(1S)$	9.0×10^{-3}	7%	33.9%	2.1×10^{-4}
$3^3P_1 \to 2^3D_2 \to 2^3P_1 \to \Upsilon(2S)$	8.0×10^{-3}	50%	11.5%	4.6×10^{-4}
$3^3P_1 \to 2^3D_2 \to 2^3P_2 \to \Upsilon(2S)$	8.0×10^{-3}	16%	11.0%	1.4×10^{-4}
$3^3P_1 \to 2^3D_2 \to 2^3P_1 \to \Upsilon(1S)$	8.0×10^{-3}	50%	8.1%	3.2×10^{-4}
$3^3P_1 \to 2^3D_2 \to 2^3P_2 \to \Upsilon(1S)$	8.0×10^{-3}	16%	9.5%	1.2×10^{-4}
$3^3P_1 \to 2^3D_2 \to 1^3P_1 \to \Upsilon(1S)$	8.0×10^{-3}	17%	33.9%	4.6×10^{-4}
$3^3P_1 \to 2^3D_2 \to 1^3P_2 \to \Upsilon(1S)$	8.0×10^{-3}	5%	19.1%	4.8×10^{-5}

TABLE VIII: Two-photon decay chains of 4^3S_1. The combined branching fractions of the chain are defined by $\mathcal{B} = \mathcal{B}_1 \times \mathcal{B}_2$ with $\mathcal{B}_1 = \mathcal{B}[4^3S_1 \to 3^3P_J\gamma]$, and $\mathcal{B}_2 = \mathcal{B}[3^3P_J \to m^3S_1\gamma]$.

Decay chain	$\mathcal{B}_1(10^{-4})$	$\mathcal{B}_2(10^{-2})$	$\mathcal{B}(10^{-6})$
$4^3S_1 \to 3^3P_2 \to 1^3S_1$	2.1	3.3	6.9
$4^3S_1 \to 3^3P_1 \to 1^3S_1$	2.4	5.4	13
$4^3S_1 \to 3^3P_0 \to 1^3S_1$	1.7	0.075	0.13
$4^3S_1 \to 3^3P_2 \to 2^3S_1$	2.1	2.7	5.7
$4^3S_1 \to 3^3P_1 \to 2^3S_1$	2.4	4.8	12
$4^3S_1 \to 3^3P_0 \to 2^3S_1$	1.7	0.010	0.017
$4^3S_1 \to 3^3P_2 \to 3^3S_1$	2.1	4.4	9.2
$4^3S_1 \to 3^3P_1 \to 3^3S_1$	2.4	8.8	21
$4^3S_1 \to 3^3P_0 \to 3^3S_1$	1.7	0.032	0.054